A Comparative Study of Observed Northern Hemisphere Circulation Statistics Based on GFDL and NMC Analyses. Part I: The Time-Mean Fields

NGAR-CHEUNG LAU

Geophysical Fluid Dynamics Program, Princeton University, Princeton, NJ 08540

ABRAHAM H. OORT

Geophysical Fluid Dynamics Laboratory/NOAA, Princeton University, Princeton, NJ 08540

(Manuscript received 5 December 1980, in final form 19 March 1981)

ABSTRACT

Two sets of monthly mean analyses based essentially on the same observational data, but employing different analysis procedures, are compared. The first set was compiled at the Geophysical Fluid Dynamics Laboratory and consists of horizontal interpolations of monthly averaged circulation statistics accumulated at individual rawinsonde stations. The second set was derived from twice-daily gridded analyses produced by the National Meteorological Center on an operational basis. The data used cover nine winters and nine summers within the 1963–73 period. The spatial domain extends in latitude from 20°N to 90°N, and in the vertical from 850 to 100 mb. The circulation statistics examined include 1) hemispheric distributions of 9-year averages as well as month-to-month standard deviations for the horizontal wind components and geopotential heights at 850, 500 and 200 mb, and the temperature at 850 mb; and 2) latitude-height sections for the zonally averaged wind and temperature, the standing eddy variances of zonal and meridional wind components, geopotential height and temperature, and the meridional transports of westerly momentum, geopotential energy and heat by standing waves.

Over certain data-sparse regions, the two analyses are further compared with actual values reported in *Monthly Climatic Data for the World* by the few rawinsonde stations located in those regions.

The time-mean fields in the two data sets are found to be generally in excellent agreement over the North American and Eurasian continents, where a dense observing network exists. The deviations between the data sets are large over the oceans and northern Africa, where the GFDL analyses give relatively weaker zonal wind speeds in the jet exit regions, stronger ageostrophic motions in the meridional direction, lower temperatures in the subtropical lower troposphere, and higher temperatures above the subtropical tropopause. The maximum local deviations are on the order of 10–15 m s^{-1} for zonal wind, 6–8 m s^{-1} for meridional wind, 50–70 m for geopotential height, and 2–4°C for temperature. These discrepancies are associated with much weaker standing eddy kinetic energy, and much stronger equatorward transports of geopotential energy by the stationary waves in the GFDL analyses. The intermonthly variability of the monthly mean fields in the GFDL set is generally weaker over the oceans.

The spatial correlation coefficients for the monthly mean fields in the two data sets do not exhibit any discernible trends during the 9-year period. This suggests that the procedural changes in the NMC analysis system during this period did not result in serious inhomogeneities in the time series of the NMC fields.

1. Introduction

The advent of the modern rawinsonde network during the late 1940's gave a strong impetus to the efforts of putting our understanding of the atmospheric general circulation on a firm observational basis. Several projects aimed at the exploitation of surface and upper air data collected by this operational network were soon initiated. A substantial fraction of these observational general circulation studies are concerned with the spatial dependence of various atmospheric parameters. This often involves the transformation of observed values taken at an irregular array of stations to a regular mesh grid. Difficulties arise over data sparse areas such as the oceans and other remote regions. These data gaps exist even in the middle latitudes of the Northern Hemisphere, as is evident from Fig. 1, which shows the distribution of reporting rawinsonde stations during a typical month in the early 1970's.

The schematic chart in Fig. 2 illustrates how the above problem may be handled by two basically different data processing procedures. These two alternative schemes, which constitute the basic framework for compiling most of the existing data sets in general circulation studies, may be briefly described as follows.

0027-0644/81/071380-24$10.00

a. Scheme A

The desired statistics are compiled at individual reporting stations for a sufficiently long period, such as a month or a season, and the horizontal fields of these statistics are then mapped onto a suitable grid. Prior to the era of automated data processing, the latter step generally involves subjective hand analysis. Since the 1960's, objective analysis techniques utilizing digital computers have been employed.

In this scheme, the quantities to be analyzed are circulation statistics accumulated at the sites of individual stations. Generally, there exists no physical basis for making *a priori* assumptions on how various patterns should behave in the data-sparse regions. In order to devise an initial-guess field for the objective analysis step, one often resorts to smoothed quantities such as the zonal or areal average of the available station data. For those long-term averaged statistics with rather smooth patterns, such choices for the first-guess field are probably reasonable. However, the analyzed pattern over the no-data areas would largely reflect the zonal or areal mean conditions, and any actual extremum values there would not be detected.

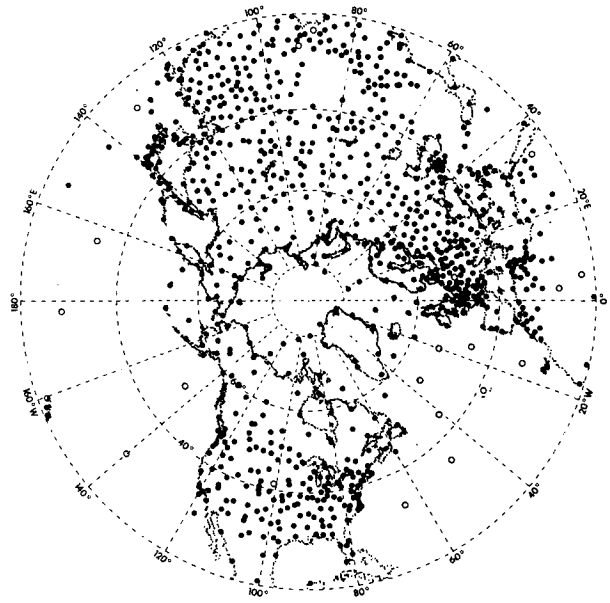

FIG. 1. Distribution of reporting rawinsonde stations during the month of January 1971. The stations chosen for checking against GFDL and NMC analyses are marked by open circles. Refer to Table 1 for details.

b. Scheme B

At regular time intervals, such as every 12 h, synoptic charts are constructed by analyzing the observations of the current atmospheric circulation on a regular grid. The desired statistics are then obtained by processing the gridded data for a long series of these charts. The synoptic analyses are often by-products of the forecast procedures at most operational weather centers, which typically consist of repetitive forecast-analysis-forecast cycles. In these cycles, the numerical prediction model makes use of the gridded synoptic data to generate the forecast for the next synoptic time, which is in turn modified by objectively inserting new observations. The updated version then serves as new initial conditions for the next forecast phase of the cycle.

In this scheme, the initial-guess fields for the objective analysis of synoptic reports are the model-generated forecasts. Through this process new information is continuously fed into the data-sparse regions. The usefulness of such information depends, of course, on the performance of the operational models. This scheme also allows for the routine incorporation of dynamical constraints such as hydrostatic balance and gradient wind balance into the first guess for instantaneous temperature, pressure and motion fields. These constraints are useful for estimating certain aspects of the circulation in data-sparse regions. For instance, one may infer the wind field in such a region from the pressure gradients prescribed by observations surrounding that region. However, the same constraints also result in systematic bias. For instance, by making use of the gradient wind equation or the balance equation in the first guess, the ageostrophic component of the flow over data-sparse regions would be significantly underestimated. On the other hand, Scheme A is not affected by such deficiencies, since it strictly adheres to observed data alone.

In addition to the upper air soundings collected by the rawinsonde stations, the observational data base for Scheme B can be extended to include wind vectors inferred from satellite imagery and occasional reports from aircraft and ships of opportunity. However, those rawinsonde soundings which are not available in an operational time frame would be excluded from the analysis in Scheme B, whereas such late reports could still be processed in Scheme A. The data inventory and the data handling procedures in Scheme A can generally be documented in detail. In Scheme B, as a result of the time constraints in most operational centers, the procedural changes in the forecast-analysis systems as well as the handling of input data (particularly "bogus" data) are usually not as well documented.

Examples of observational studies utilizing data compilations based on earlier versions of Scheme A (using subjective analyses) may be found in the voluminous works by V. P. Starr and his coworkers of the Planetary Circulations Project at the Massa-

chusetts Institute of Technology (MIT).[1] These efforts were continued at Environmental Research and Technology, Inc. (ERT), for describing the water cycle (see e.g., Peixóto *et al.*, 1978). Various versions of Scheme A were also used by Crutcher (1959)[2] and Crutcher and Meserve (1970)[3] for constructing climatological charts of the Northern Hemisphere, by Oort and Rasmusson (1971) at the Geophysical Fluid Dynamics Laboratory (GFDL) for documenting zonally averaged circulation statistics north of 10°S, and by Newell *et al.* (1972, 1974) at MIT for examining the circulation of the tropical and subtropical atmospheres. These sets of analyzed circulation statistics have laid the groundwork for a variety of observational studies. Such studies include the variability and annual cycle of the atmospheric energetics by Peixoto and Oort (1974) and Oort and Peixóto (1974, 1976), the ocean-atmosphere heat balance by Oort and vonder Haar (1976), the momentum and kinetic energy balances of the tropics by Oort and Chan (1977), the local balances of kinetic energy and vorticity by Holopainen (1978a, b), and the hemispheric distribution of diabatic heating rates by Geller and Avery (1978). More recently, a comprehensive collection of global circulation statistics has been archived at GFDL by processing the radiosonde soundings for the 15-year period from 1958 to 1973. Part of this data set will be published in the form of microfiches (Oort, 1981).[4]

The analyzed products of various versions of Scheme B have been used by Klein (1951) for studying the daily pressure variability, by Clapp (1956) for examining various components of the vorticity balance, by Wiin-Nielsen (1959), Wiin-Nielsen *et al.* (1963, 1964), Brown (1964), and Krueger *et al.* (1965) for studying atmospheric energetics, by Haines and Winston (1963) for analyzing heat transport processes, by van Loon *et al.* (1973) for describing the structure of planetary-scale standing waves, and more recently, by Blackmon (1976), Blackmon *et al.* (1977) and Trenberth (1979) for examining the local features of the general circulation. Over the years, R. L. Jenne and his associates at the National Center for Atmospheric Research (NCAR) have made a sustained effort to archive the twice-daily analyses produced by the U.S. National Meteorological Center (NMC), and to consolidate these data grids in a tape library for meteorological research.[5] By making use of these NMC analyses for 11 winter seasons, Lau (1978) has compiled a set of mean, temporal variance and covariance circulation statistics. This data set forms the basis for a series of investigations on the regional characteristics of the Northern Hemisphere wintertime circulation (e.g., Lau, 1979a, b; Lau and Wallace, 1979; Blackmon and Lau, 1980). G. H. White of the University of Washington has recently documented a parallel set of the summertime circulation statistics. A selection of the NMC statistics for both seasons will shortly appear as an NCAR technical note (Lau *et al.*, 1981).

As these different general circulation data sets come into popular usage in various sectors of the meteorological community, we feel that the opportune moment has arrived for an extensive comparison between the products of two independent compilation projects in which we were heretofore separately involved. As was mentioned earlier, the first project was undertaken at GFDL, and made use of Scheme A to process upper air soundings at individual rawinsonde stations (Oort and Rasmusson, 1971); the second project was accomplished at the University of Washington and NCAR, and made use of Scheme B to process the twice-daily NMC synoptic analyses (Lau, 1978). We anticipate that the findings reported here should be helpful to present and future users of these long-term sets. The general impressions we gain should also serve as useful guidelines for research strategies in diagnosing the hierarchy of data sets for the Global Weather Experiment, for initialization and verification procedures associated with numerical weather prediction models, and for comparisons of climate simulations by general circulation models against observations.

The uncertainties of the circulation statistics in various data sets over the data-sparse regions have already been the subject of several investigations. Holopainen (1968) has noted that the estimates of the geostrophic zonal wind and the meridional flux of zonal momentum over the central Pacific based on NMC analyses are substantially larger than the corresponding values based on more conventional interpolations of station data. Mak (1978) has demonstrated that daily analyses prepared by the Canadian Meteorological Center yield stronger standing eddy momentum fluxes at 500 mb than those reported by Oort and Rasmusson (1971) and Newell *et al.* (1972, 1974). By making use of the output of the ZODIAC general circulation model developed at GFDL (Manabe and Holloway, 1975), Oort

[1]Most of these works are collected in Starr, V. P., and B. Saltzman, Eds., 1966: *Observational Studies of the Atmospheric General Circulation*. Sci. Rep. 2, Planetary Circulation Project, MIT, 700 pp.

[2]Crutcher, H. L., 1959: *Upper Wind Statistics Charts of the Northern Hemisphere*, Vols. 1 and 2. NAVAER 50-1C-535, Office of the chief of Naval Operations, Washington DC.

[3]Crutcher, H. L., and J. M. Meserve, 1970: *Selected Level Heights, Temperatures and Dew Points for the Northern Hemisphere*. NAVAIR 50-1C-52 [Govt. Printing Office].

[4]Oort, A. H., 1981: *Global Atmospheric Circulation Statistics, 1958–1973*. NOAA Prof. Pap. (in preparation).

[5]Jenne, R. L., 1975: Data sets for meteorological research. NCAR Tech. Note TN/IA-111, 194 pp.

(1978) compared two sets of zonally and areally averaged circulation statistics. One of these sets was based on the full model grid, and the other set was based on a simulated network reflecting the existing distribution of rawinsonde stations. When averaged over the Northern Hemisphere, the root-mean-square errors associated with spatial data gaps for the zonal and meridional wind speeds, geopotential height and temperature were 2–5m s^{-1}, 1–2 m s^{-1}, 10–25 m and 0.5–1°C, respectively. Rosen and Salstein (1980) recently computed statistics by using both conventional station data and the NMC global Hough analyses for the 1976–77 winter. They concluded that a good agreement exists between the estimates by the two data sets on the zonally averaged eddy transports of momentum and heat in the middle latitudes. It was also noted that, since the Hough analyses do not contain any zonal mean meridional circulation, they generally yield unrealistic transports in the tropics. Arpe (1980)[6] examined the objective analyses for February 1976 produced by the operational weather centers in the United States, Germany and the United Kingdom. Large systematic deviations were noted between different analyses over the data-sparse regions. These discrepancies led to noticeable differences in the estimates of static stability as well as kinetic and available potential energy.

The results of this comparative study are to be presented in two parts. Part I is devoted to the structure of the time mean fields. The spatial distributions of the temporal variance and covariance statistics, as well as the atmospheric energy cycle, will be treated in Part II. In Section 3 of this first installment, the GFDL and NMC patterns for the monthly mean fields at selected levels for nine winters and nine summers are compared against each other, and against selected monthly mean data recorded in *Monthly Climatic Data for the World,*[7] most of which consist of soundings taken by weather ships or islands located over the data-sparse Atlantic and Pacific Oceans (see Fig. 1). Variations with height of the deviations between the two data sets are depicted by vertical profiles over selected geographical locations, where the sets exhibit the largest differences. Latitude-height distributions for the zonally averaged fields and standing eddy statistics are presented in Section 4. In Section 5 are shown the geographical patterns of the month-to-month variability of the fields included in Section 3. Finally, the results on temporal variations of the differences between the two sets during the 9-year period are discussed in Section 6.

2. Description of the data sets

The primary data base for Part I of this comparative study consists of the monthly mean fields of zonal and meridional wind components, geopotential height and temperature for the nine winter seasons (December, January, February) from 1963–64 to 1972–73 (except 1969–70, for which most NMC wind analyses are missing), and for the nine summer seasons (June, July, August) from 1964 to 1972. During most of this period, the data grids are available at 850, 700, 500, 400, 300, 200 and 100 mb.

The two data sets being examined are as follows:

1) The GFDL set, which is composed of objective global analyses of monthly circulation statistics accumulated at individual rawinsonde stations (see Scheme A in Fig. 2). For a given statistical parameter during a given month, the first-guess field used in the objective analysis was taken to be the zonal mean of all the available monthly-mean data for that parameter in that month. Further details on the data handling procedures are presented in Oort (1981).[4] Prior to 1968, the compilations were based on the daily upper air soundings at 0000 GMT. The data base for the 5-year period from 1968 to 1973 was expanded to include soundings at 0000 and 1200 GMT.

2) The NMC set, which is based on operational twice-daily (0000 and 1200 GMT) analyses prepared by NMC (see Scheme B in Fig. 2). The first-guess fields for the synoptic analyses of temperature and geopotential height were based on the 12 h forecasts generated by the operational prediction models (see McDonell, 1967 for details).[8] The numerics of these models are described by Shuman and Hovermale (1968). Prior to 1971, the initial winds were derived from the analyzed height fields by using the nonlinear balance equation. Starting from August 1971, the gradient wind equation was used instead (see Cooley, 1971).[9] The observations were inserted into the above initial guess fields using the objective analysis scheme designed by Cressman (1959).

The NMC wind analyses at the following levels are missing for the winter seasons listed in parentheses: 850 and 700 mb (1964–65 and 1965–66), 500 mb (1964–65), and 400 mb (1963–64 and 1964–65). At these particular levels, the comparisons are done

[6] Arpe, K., 1980: Confidence limits for verification and energetics studies. European Centre for Medium Range Weather Forecasts, Tech. Rep. No. 18, 24 pp.

[7] *Monthly Climatic Data for the World, 1963–1973,* Vols. 16–26. Sponsored by the World Meteorological Organization and ESSA [Govt. Printing Office].

[8] McDonell, J. E., 1967: A summary of the first-guess fields used for operational analyses. NMC Tech. Memo. No. 38 [National Meteorological Center, NOAA, Washington DC 20233.]

[9] Cooley, D. S., 1971: New initialization procedure for the 6-layer (PE) numerical prediction model. Tech. Proc. Bull. No. 65, 4 pp. [National Meteorological Center, NOAA, Washington DC 20233.]

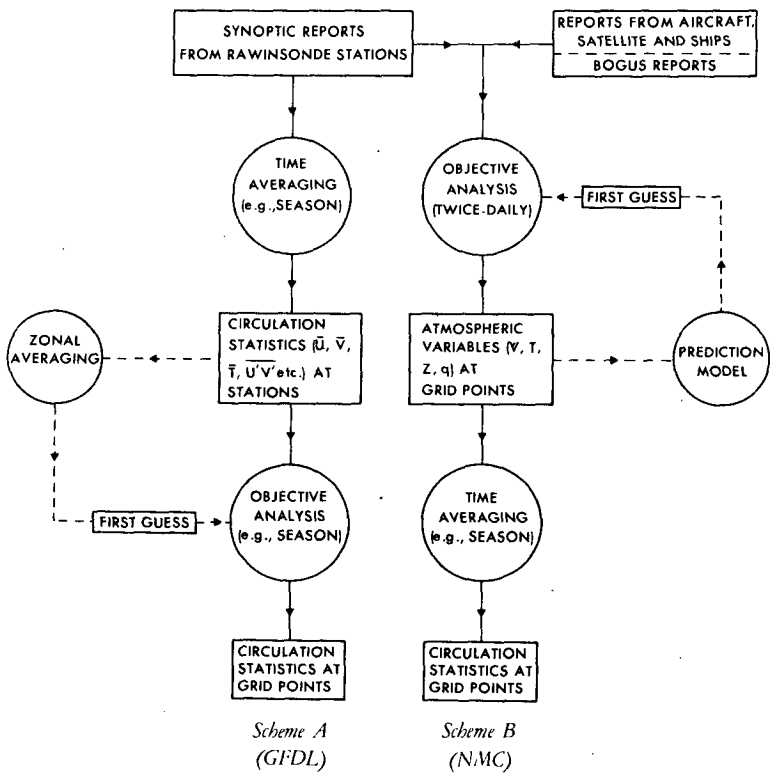

FIG. 2. Flow diagram illustrating the two alternative processing schemes for compiling general circulation statistics.

only for those winters covered by both NMC and GFDL sets. Since the NMC data set for the 1963–73 period is analyzed on an octagonal grid with coverage limited to the region north of the 20°N latitude, it is possible to perform comparisons only for that domain.

The accuracy of the GFDL and NMC data sets is further checked against the monthly mean data summaries at 22 radiosonde stations for the corresponding winter seasons. Most of these stations (indicated by open circles in Fig. 1 and listed in Table 1) are chosen by virtue of their locations in the data-sparse regions. The data records for these upper air soundings are routinely compiled and published by the U.S. National Climatic Center through the sponsorship of the World Meteorological Organization,[7] and are hereafter referred to as WMO data. For a given month at a given station, the monthly averaged values of soundings at a certain hour of day are archived. The specific hour of the day varies from station to station, and from month to month. For those stations with missing records during the nine winters covered by the present study, the data checking is done only for those months with station reports.

3. Hemispheric distributions of time-mean fields

a. Winter season

1) ZONAL WIND

Fig. 3 shows the distributions of the 9-winter means of the zonal wind component at 200 mb, as given by (a) GFDL and (b) NMC analyses. The difference between these two fields is displayed in Fig. 3c; the pair of arrows in this figure depict the positions of the Asian and North American jet streams, as given by the NMC data set (see Fig. 3b). Over a large fraction of the North American and Eurasian continents, where a dense observing network exists, the differences between the two data sets are typically less than 2–3 m s^{-1}. Large differences show up over the Pacific and Atlantic, and over the Sahara and southwestern Asia. The NMC values for the intensity of the zonal flow in the exit regions of the North American and Asian jet streams are larger than the corresponding GFDL values by as much as 10–15 m s^{-1}. Also worth noting are the relatively weaker zonal winds in the NMC analyses over the subtropical Pacific (between 120°W and 160°W) and the subtropical Atlantic. As a result,

the meridional gradients of the zonal flow intensity over the oceans are stronger in the NMC pattern. The axes of the wind-speed maxima corresponding to the two major jet streams exhibit a slight southwest-to-northeast orientation in the NMC pattern, while they are more zonally oriented in the GFDL analyses. The above results agree with a similar set of maps presented by Rosen and Salstein (1980, Fig. 5) for the 1976–77 winter. Holopainen (1968, Fig. 1) has also noted the large differences (~20 m s^{-1}) in the geostrophic zonal wind speed at 40–45°N and 160°W between the NMC and conventional station analyses for January 1964. The average differences between the NMC and GFDL data for the 9-winter period are considerably smaller (<6 m s^{-1}) over the same region.

The GFDL and NMC values for the zonal wind at the locations of the set of 22 rawinsonde stations (depicted in Figs. 1 and 3c) are obtained from the data grids by linear interpolation. These values are then checked against the station records prepared by the National Climatic Center (WMO data). The comparison is done only for those months with station reports. In Fig. 3d, the differences between the WMO data and the GFDL (NMC) analyses are displayed above (below) the sites of individual stations. It is seen from Figs. 3c and 3d that the differences among the three data sets are relatively small (<2 m s^{-1}) at most of the selected stations. Over much of the western Pacific, central Atlantic and northern Africa, the zonal wind speeds given by the GFDL set are weaker than the WMO data. This is particularly evident for the two stations lying along the axis of the Asian jet stream (Fukuoka and Ship V), where the GFDL values are smaller by 5–6 m s^{-1}. Further data checking indicates that the zonal wind speeds at stations in Japan and at Ship V are generally lower in the final GFDL analyses (Fig. 3a) than in the original input station data used for producing these analyses. This discrepancy results from the smoothing and interpolation procedures in the GFDL analysis system, which mainly affects the wind speed near the jet stream core. Over most of the oceanic areas, the NMC analyses yield slightly stronger zonal winds (by 1–2 m s^{-1}) when compared with station data.

The difference maps between the GFDL and NMC zonal wind data at other levels (not shown) display features which are qualitatively similar to those shown in Fig. 3c. The vertical profiles of the differences between these two data sets over selected patches are displayed in Fig. 4. These patches (depicted in Fig. 3d) have dimensions of 10° longitude and 5° latitude, and are chosen to represent those locations where the differences between the two data sets are largest (see Fig. 3c). As a measure of the season-to-season variability of these differences, the range between ±1 standard deviation of the seasonally averaged differences between the two sets in the 9-year record is depicted in Fig. 4 by the shaded envelopes. The deviations between the two sets for a given location tend to be of the same sign for the whole atmospheric column. The largest differences are found at the jet stream level.

TABLE 1. List of rawinsonde stations from the data summaries in the *Monthly Climatic Data for the World* chosen for checking against the GFDL and NMC analyses. The last two columns give the number of reporting months for geopotential height and temperature (left column) and for zonal and meridional wind (right column) during the nine winter seasons from 1963–64 to 1972–73 (except 1969–70). The largest possible number in these columns is 27. The locations of these stations are indicated by open circles in Fig. 1.

WMO no.	Station name	Latitude	Longitude	Number of months with reports	
				z, T	u, v
08509	Lajes, Acores	38.8°N	27.1°W	17	17
08521	Funchal, Madeira	32.6°N	16.8°W	27	6
10739	Stuttgart, Germany	48.8°N	9.1°E	27	27
42410	Gauhati, India	26.1°N	91.6°E	26	15
42809	Calcutta, India	22.6°N	88.3°E	26	21
47807	Fukuoka, Japan	33.6°N	130.3°E	27	27
47945	Minamidaitojima, Japan	25.8°N	131.1°E	19	19
60630	In Salah, Algeria	27.1°N	2.5°E	19	17
60680	Tamanrasset, Algeria	22.8°N	5.5°E	22	10
62414	Asswan, Egypt	24.0°N	32.8°E	22	16
72562	North Platte, Nebraska, U.S.	41.1°N	100.6°W	27	27
78016	St. George's, Bermuda	32.3°N	64.6°W	21	9
91066	Midway Island	28.1°N	177.3°W	25	18
91165	Kauai, Hawaii	22.0°N	159.3°W	27	27
99008	Ship C	52.8°N	35.5°W	26	25
99009	Ship D	44.0°N	41.0°W	26	26
99010	Ship E	35.0°N	48.0°W	26	26
99015	Ship J	52.5°N	20.0°W	26	25
99016	Ship K	45.0°N	16.0°W	23	19
99019	Ship N	30.0°N	140.0°W	26	26
99021	Ship P	50.0°N	145.0°W	21	19
99027	Ship V	34.0°N	164.0°E	21	20

2) MERIDIONAL WIND

The GFDL and NMC patterns for the time-averaged meridional wind at 200 mb, and the corresponding difference map, are shown in Figs. 5a–5c. The locations of the maxima and minima in Figs. 5a and 5b are in good agreement. The analyses over northeastern China,[10] central Pacific and western

[10]It should be noted here that, during the earlier half of the 9-year period considered in this study, the number of reporting stations over China is much less than that indicated in Fig. 1.

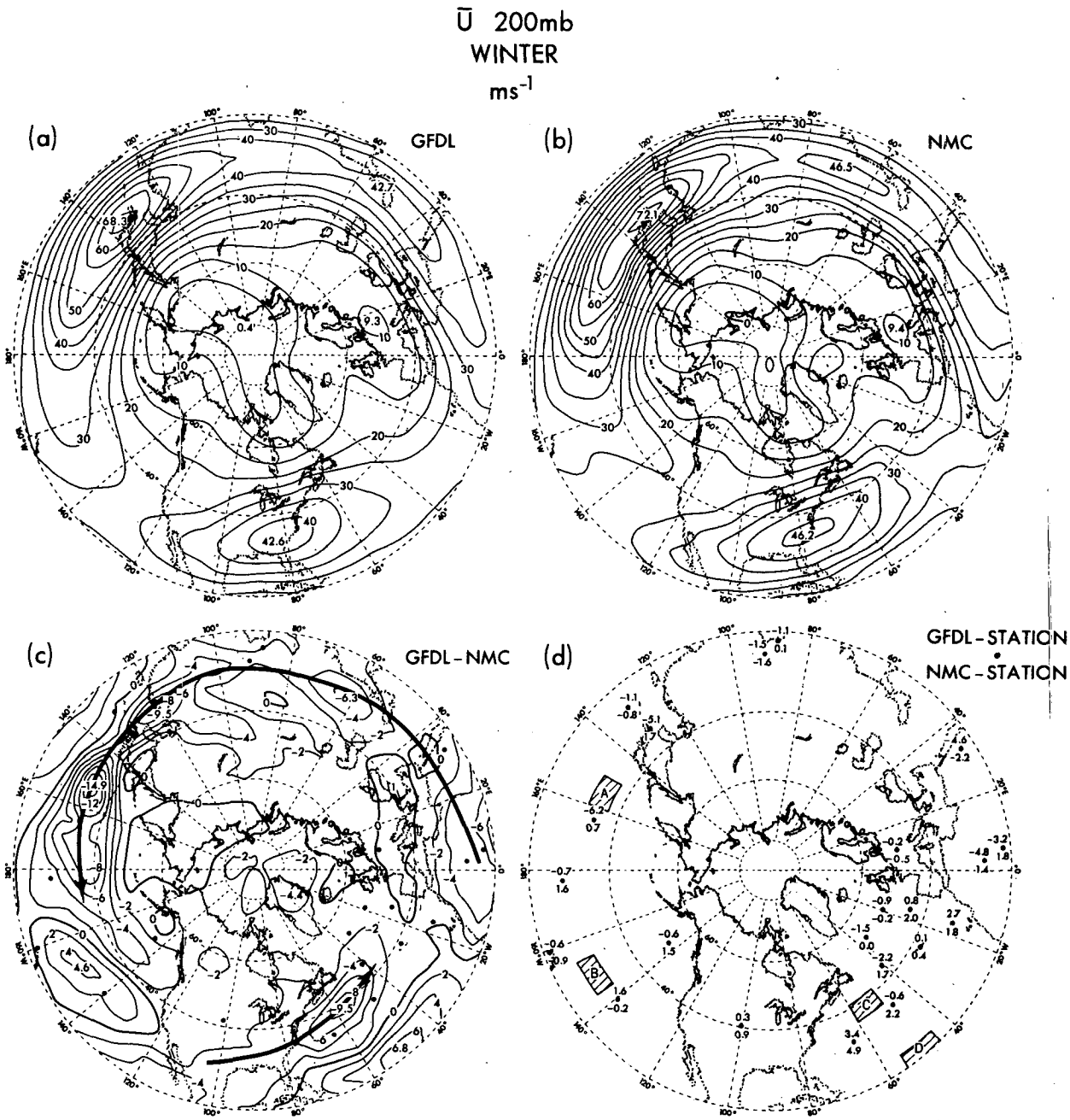

FIG. 3. Distributions of the 9-winter average of the zonal wind (m s^{-1}) at 200 mb, based on (a) GFDL analysis and (b) NMC analysis. The difference map in (c) shows the pattern obtained by subtracting the NMC analysis from the GFDL analysis. The arrows depict the positions of the two principal wintertime jet streams as inferred from the NMC analysis. The dots indicate the locations of rawinsonde stations chosen for checking against the GFDL and NMC analyses. The values obtained by subtracting the WMO data from the GFDL (NMC) analyses are displayed above (below) the sites of individual stations in (d). The shaded patches indicate those regions for which vertical profiles of the deviations between the GFDL and NMC analyses are to be presented.

Atlantic are quite different. These regions coincide with the zones for transition from northerly to southerly flows or vice versa. The difference also is large over parts of northern Africa, where the meridional flows in the two sets are opposite in sign.

The GFDL and NMC analyses for meridional wind are checked against the WMO reports in Fig. 5d. The differences at most of the stations are less than 1–2 m s^{-1}. The NMC analyses deviate substantially from the WMO reports for Ship V, Midway and Bermuda (3–6 m s^{-1}), and for several land stations near the 20°N latitude (up to 10 m s^{-1}),

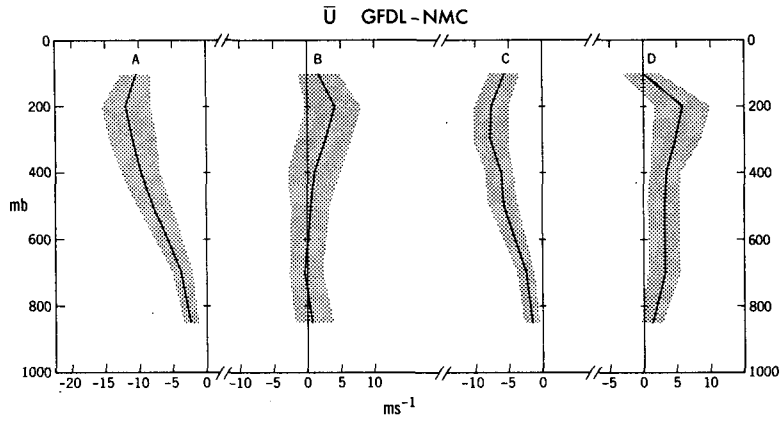

FIG. 4. Vertical profiles of the differences in zonal wind speed (m s^{-1}) between the two analyses (GFDL minus NMC) averaged over the individual patches shown in Fig. 3d. The shaded envelopes depict the range between ±1 standard deviation of the seasonally averaged differences between the two data sets during the 9-year period.

which corresponds roughly to the edge of the integration domain of the NMC models.

Five patches with sides of 15° longitude and 7.5° latitude are selected over the regions associated with largest differences between the GFDL and NMC sets (Fig. 5d). The vertical profiles of the means and standard deviations of these differences for the individual patches are presented in Fig. 6. The differences over a given location tend to be of one sign and exhibit a maximum at 200 mb.

3) GEOPOTENTIAL HEIGHT

The distributions of the geopotential height at 500 mb based on GFDL and NMC analyses are shown in Figs. 7a and 7b, respectively. The differences between these two patterns are shown as contours in Fig. 7c. There is good agreement between the two data sets over regions with dense observing networks. The differences over the oceans are large (up to 50–60 m). Superimposed on the contours in Fig. 7c are arrows depicting the local difference between the vector wind field in the two analyses at 500 mb. It is seen that the differences in the height and horizontal wind fields at this level tend to be in geostrophic balance in middle latitudes. Both GFDL and NMC sets compare well against the available WMO reports (Fig. 7d). With a few exceptions, notably the land stations near 20°N, the deviations shown in Fig. 7d are <10 m.

In Fig. 8 are shown the differences in geopotential height (contours) and in the horizontal vector wind field (arrows) between the two analyses, at (a) 200 mb and (b) 850 mb. If the arrows and the contours at 200 mb were to satisfy the geostrophic relationship, the former would have a less southerly component over China and northern Africa, and a less northerly component over the Pacific and western Atlantic than is actually indicated in Fig. 8a. The reverse situation appears to hold at 850 mb (Fig. 8b).

It was proposed by Namias and Clapp (1949) and Blackmon *et al.* (1977), among others, that local, thermally direct meridional circulations prevail over the entrance regions of the jet streams (i.e., eastern Asia, southern United States and northern Africa). The ageostrophic flow associated with these circulations is directed poleward near the tropopause level, and equatorward in the lower troposphere. On the other hand, the oceanic regions lying downstream of the jet maxima are characterized by thermally indirect circulations, with the pattern of ageostrophic flow being the opposite of that in the entrance regions. It is seen that the meridional component of the arrows in Fig. 8 tends to be oriented in the same sense as the above ageostrophic circulations at the respective locations. For instance, the arrows in the entrance region of the Asian jet stream (at 110°E between 25 and 40°N) have a strong poleward component at 200 mb (Fig. 8a). The arrows and contours in that region evidently do not satisfy the geostrophic relationships, since the contour field over eastern Asia is characterized by far too weak gradients. Conversely, the arrows in the exit region of the Asian jet stream (at 170°E between 25° and 40°N) have a distinct equatorward component at 200 mb and are directed across the local contours. These features suggest that the estimates by the NMC analyses on the intensity of the local ageostrophic flow are relatively lower than the corresponding GFDL values. Since the NMC wind analyses make routine use of the balance equation or the gradient wind equation to obtain the first-guess field, it is anticipated that they would

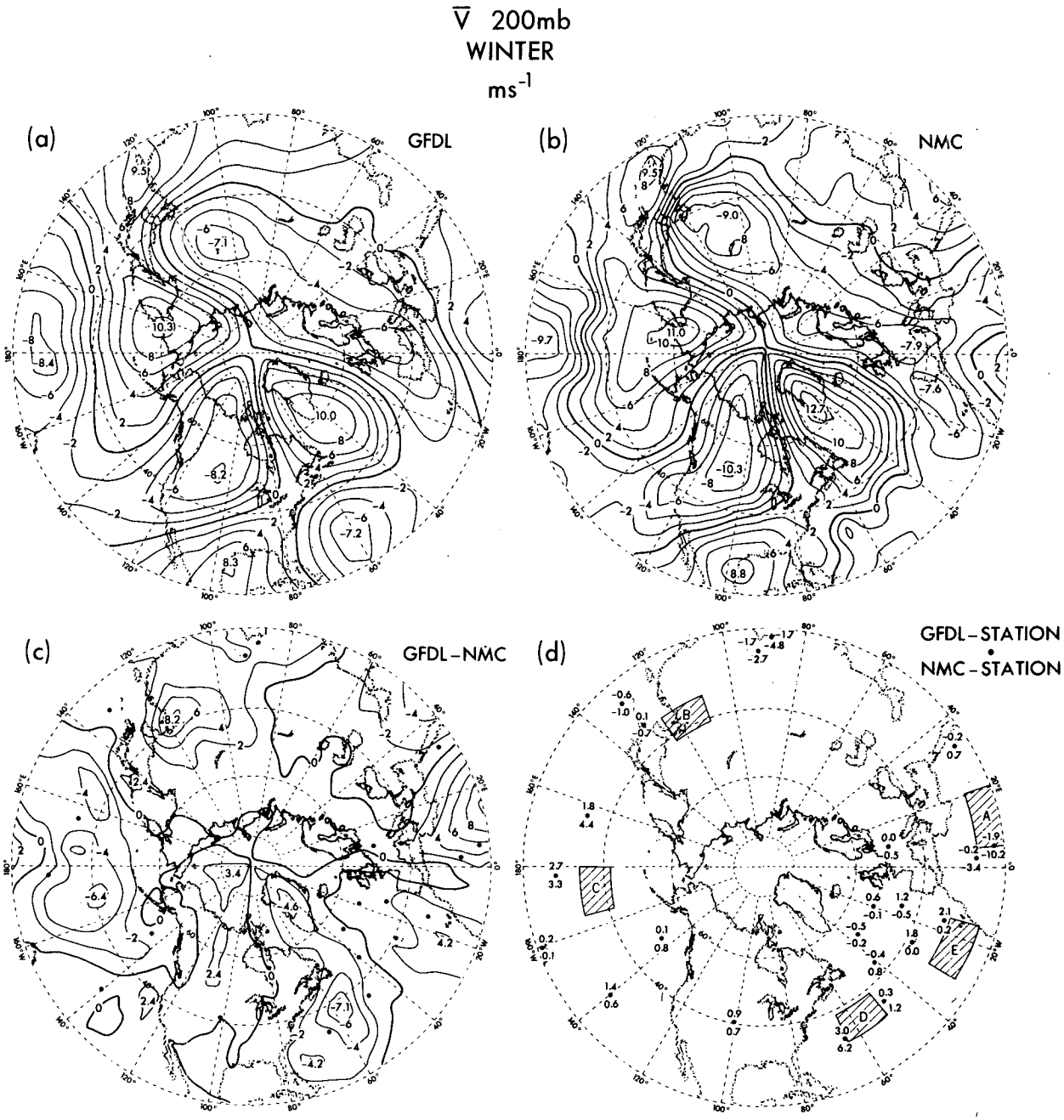

FIG. 5. As in Fig. 3 except for meridional wind speed at 200 mb.

systematically underestimate the ageostrophic component of the motion field. This probably makes a substantial contribution to the large differences between the meridional wind speeds in the two analyses over the entrance and exit regions of the jet streams (Fig. 5c).

It is evident from Figs. 7c and 8 that the difference patterns for geopotential height are qualitatively similar throughout the troposphere. The profiles of the differences between the GFDL and NMC analyses averaged over selected patches (see Fig. 7d) are displayed in Fig. 9. Largest deviations (up to 70 m) occur at 200 and 300 mb.

4) TEMPERATURE

The GFDL and NMC analyses for temperature at 850 mb are shown in Figs. 10a and 10b. These fields are compared with each other in Fig. 10c, and with the WMO reports in Fig. 10d. With a

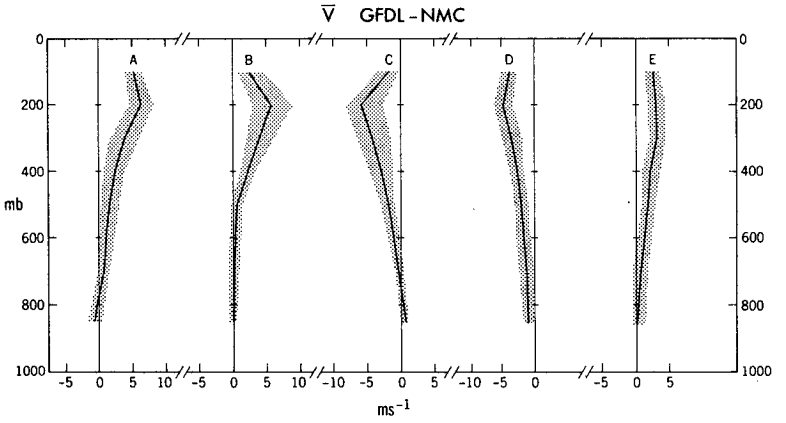

FIG. 6. As in Fig. 4 except for meridional wind speed averaged over the individual patches shown in Fig. 5d.

few exceptions, the NMC analyses at 850 mb give maritime temperatures which are up to 4°C higher than the corresponding GFDL analyses. Comparing the features in the difference map for temperature in the lower troposphere and the vertical profiles for deviations in geopotential height (Fig. 9), one finds that they are consistent as far as hydrostatic balance is concerned. The differences between the two sets and the WMO reports are much smaller (mostly less than 1°C). Over much of the oceans, the NMC analyses of the temperature field give values which are systematically higher than the corresponding WMO reports.

The vertical profiles of the differences between the GFDL and NMC sets (Fig. 11) indicate that, while the NMC temperatures are higher than the corresponding GFDL values over much of the subtropical oceans in the lower troposphere, the reverse is true at the 100 and 200 mb levels. This implies that, over the subtropical oceans, the mid-tropospheric static stability computed using GFDL analyses is higher than that derived from NMC analyses.

b. Summer season

The time-mean fields of the GFDL and NMC data sets for summer have been compared in a manner analogous to that outlined for winter. Since most of the findings for both seasons are qualitatively similar, the presentation of the summer results in this subsection is confined to difference maps for zonal and meridional wind at 200 mb, geopotential height at 500 mb, and temperature at 850 mb. These maps are shown in Figs. 12a–12d.

The solid arrows in the difference maps for zonal wind (Fig. 12a) depict the positions of the summertime jet streams, as inferred from the axes of maxima (>20 m s^{-1}) in the NMC analyses of zonal wind (not shown). It is seen that the GFDL set gives relatively weaker zonal flows along the major jet axes. The large discrepancies between the two sets over the Pacific is a reflection of the tendency for the jet stream in the NMC set to extend further eastward into the Pacific. The wind speeds in the GFDL set are larger on the southern flank of the jet streams. Since the locations of the jet axes in the GFDL pattern essentially coincide with those in the NMC pattern, the NMC analyses give stronger lateral shears of the time mean flow on the anticyclonic side of the jets over the mid-oceans. The difference map for meridional wind at 200 mb (Fig. 12b) indicates that the two data sets exhibit large deviations (up to 3–5 m s^{-1}) over the two oceans and along the zonal belt between 20 and 30°N. The differences between the geopotential height field in the two analyses at 500 mb also attain maximum values over the oceans (Fig. 12c). In Fig. 12d is shown the difference map for temperature at 850 mb. Except for the maritime regions off the west coasts of North America and northern Africa, the NMC analyses portray a relatively warmer troposphere over the zonal belt between 20 and 40°N.

4. Latitude-height distributions of zonally averaged wintertime statistics

In this section the GFDL and NMC patterns for mean, standing eddy variance and covariance statistics are presented in latitude-height sections. In the present study, the standing eddy variance and covariance statistics for each winter are first computed on the basis of seasonally averaged data, and the 9-winter averages of these statistics are then taken. The differences between the two sets are to be examined in light of the hemispheric maps for the relevant fields presented in the previous section.

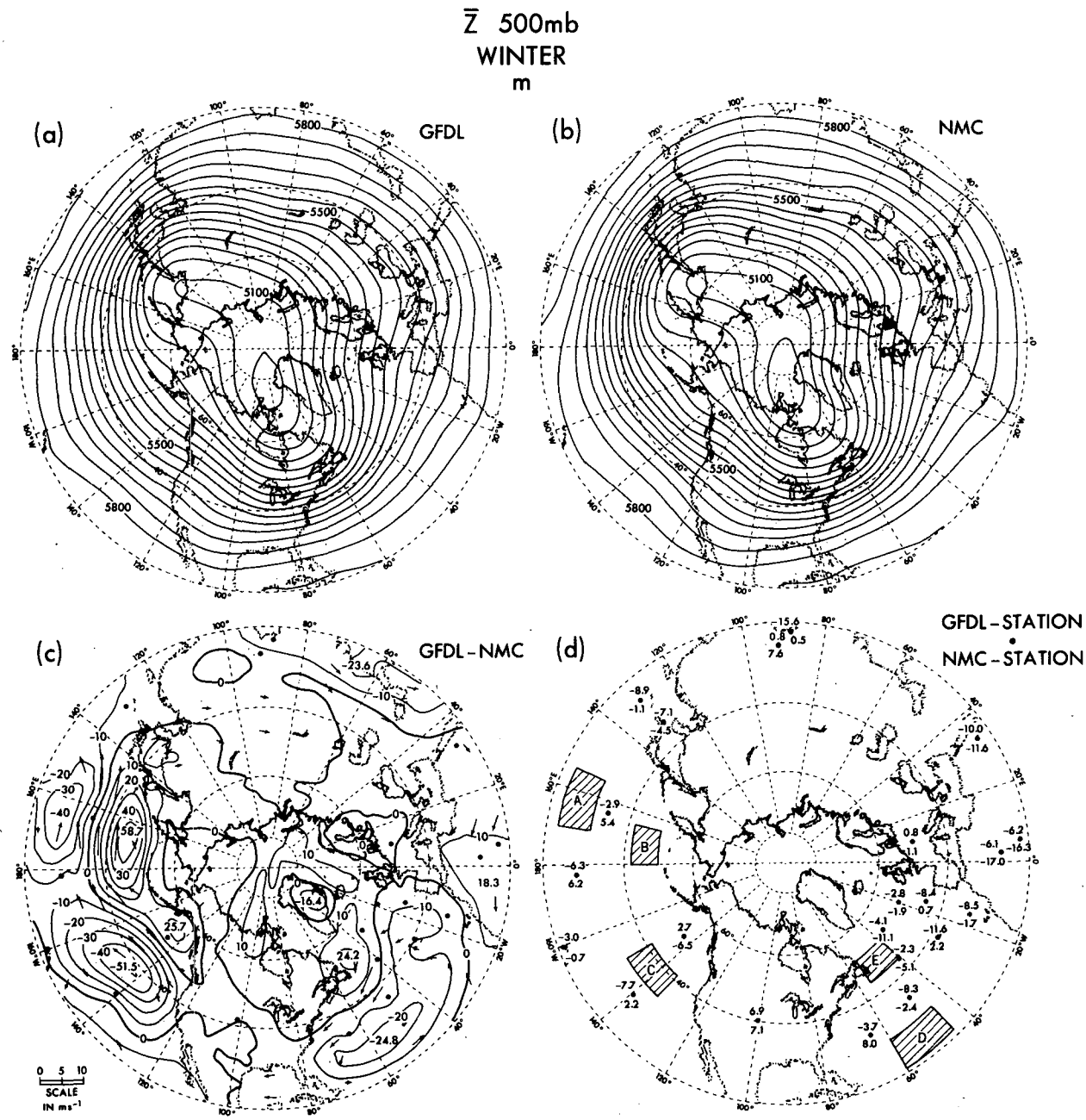

FIG. 7. As in Fig. 3 except for geopotential height (m) at 500 mb. The arrows in Fig. 7c represent the difference between the two analyses (GFDL minus NMC) in the horizontal vector wind field at 500 mb. The length scale for the arrows is given at the lower left-hand corner. Arrows which are too small to show up clearly have been omitted.

The symbols to be used here are defined as follows:

$$\bar{X} = \frac{1}{T}\int_0^T X dt \qquad \text{(time average)}$$

$$[X] = \frac{1}{2\pi}\int_0^{2\pi} X d\lambda \qquad \text{(zonal average)}$$

$$X^* = X - [X] \begin{pmatrix}\text{deviation from}\\ \text{zonal average}\end{pmatrix}.$$

Here t is time and λ longitude.

a. Mean statistics

In Fig. 13 is shown the zonally averaged distributions of the (a) zonal wind, (b) meridional wind

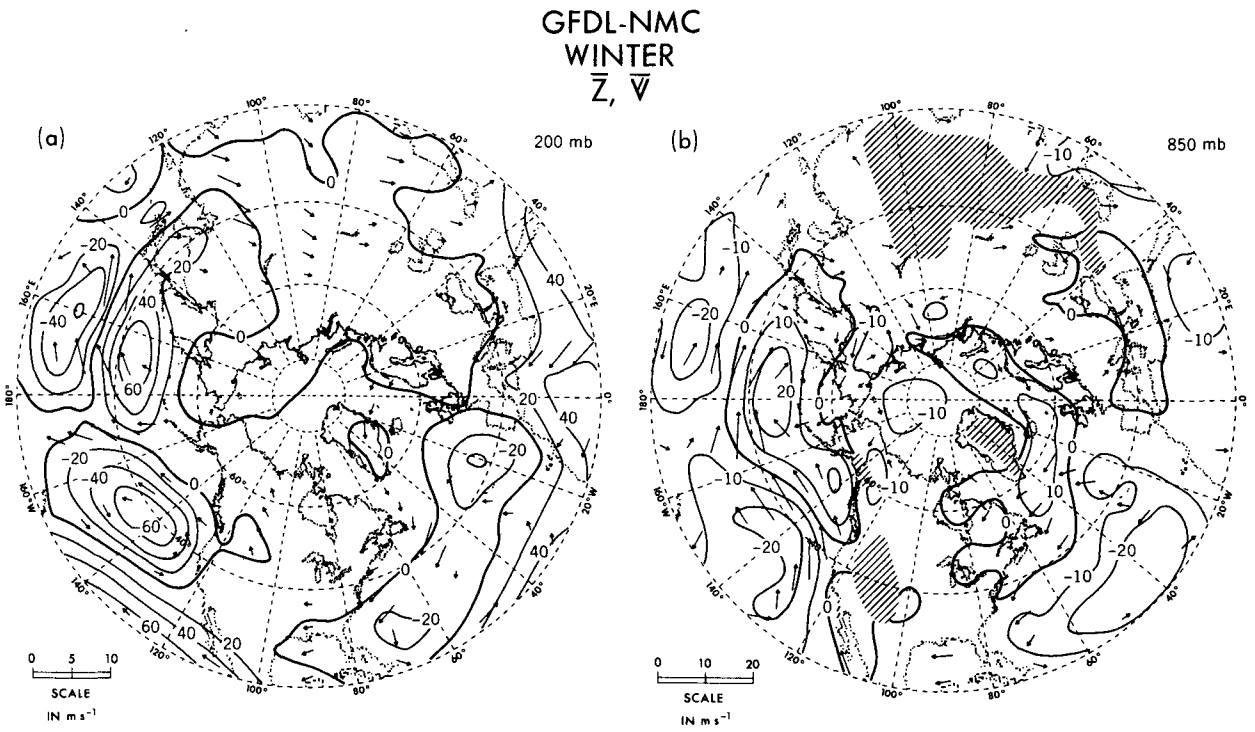

FIG. 8. As in Fig. 7c except for (a) 200 mb and (b) 850 mb. Note that a different length scale (shown at the lower left-hand corner) for the arrows is used for each map. The shaded areas in (b) indicate topographic heights > 1500 m.

and (c) temperature. For each parameter, the patterns corresponding to GFDL analysis, NMC analysis, and the difference between the two data sets are displayed in the left, middle and right panels, respectively.

1) ZONAL WIND

The flow intensity as deduced from the GFDL analysis is relatively weaker (by 1–3 m s^{-1}) in the vicinity of the zonal mean jet (Fig. 13a). This can be accounted for by the weaker zonal flows in the GFDL set over the oceans (Fig. 3). The patterns in Fig. 13a agree with the results presented by Rosen and Salstein (1980, Fig. 4), who have made a similar comparison for the 1976–77 winter. The findings by Oort (1978, Fig. 5) using the history tapes of a GFDL general circulation model also indicate that the analysis based on a simulated rawinsonde network tends to underestimate the zonally averaged flow.

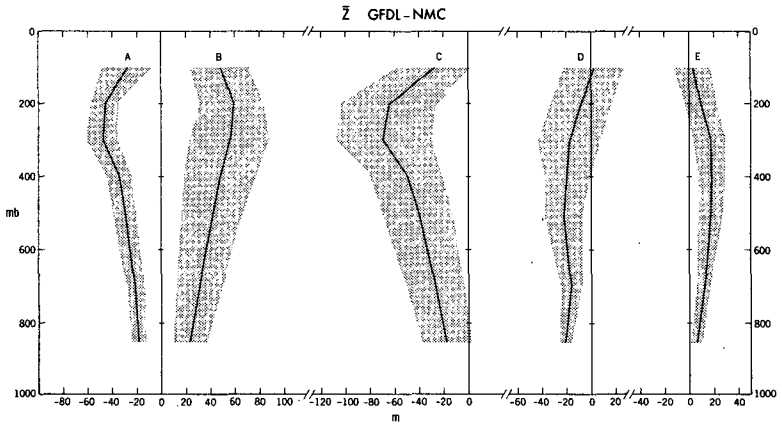

FIG. 9. As in Fig. 4 except for geopotential height (m) averaged over the individual patches shown in Fig. 7d.

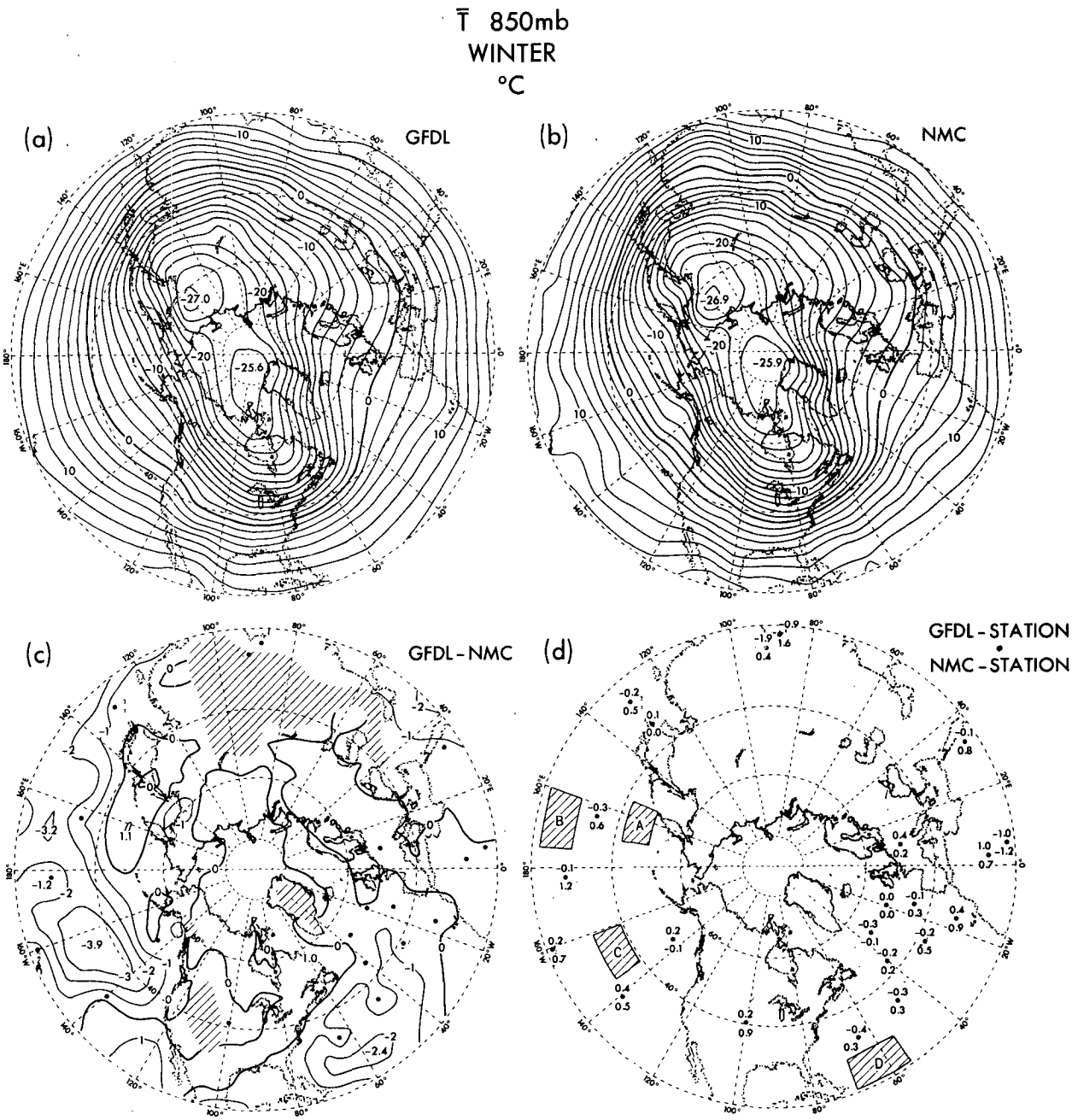

FIG. 10. As in Fig. 3 except for temperature (°C) at 850 mb. The shaded areas in (c) indicate local topographic heights > 1500 m.

2) MERIDIONAL WIND

The NMC analysis for meridional wind yields a Ferrel cell in the middle latitudes which is weaker and displaced further poleward when compared with the GFDL pattern (Fig. 13b). The northern tip of the Hadley circulation (between 20 and 30°N) is much more prominent in the GFDL set. It is worth noting that the objective analysis scheme designed by Cressman (1959) was in effect in the NMC forecast operations during the entire period (1963–73) covered by this study. This scheme does not constrain the zonally averaged meridional flow to be zero, as is in the case of the Hough analysis scheme introduced in 1974 (Rosen and Salstein, 1980, Section 5.1).

3) TEMPERATURE

The comparison of the zonally averaged temperature fields (Fig. 13c) reaffirms the observation pertaining to Fig. 10 that, equatorward of ~45°N, the

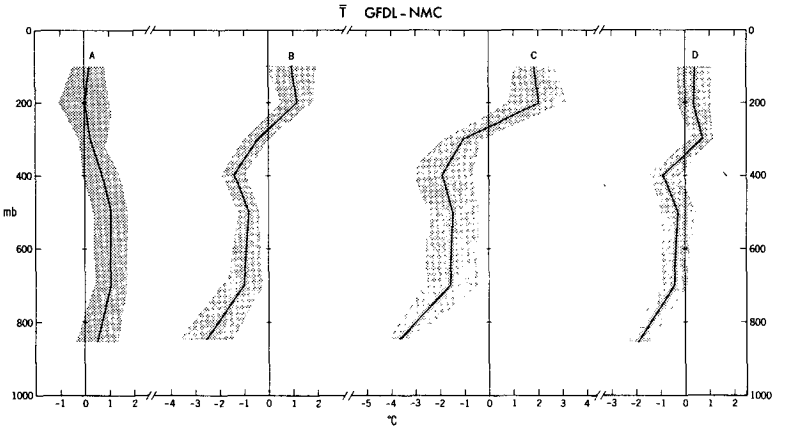

FIG. 11. As in Fig. 4 except for temperature (°C) averaged over the individual patches shown in Fig. 10d.

NMC temperature analyses give relatively higher values below 300 mb, and lower values above this level. The pattern further suggests that the reverse situation applies to the high latitudes. Similar differences are also implicit in the corresponding cross sections presented by Rosen and Salstein (1980, Fig. 11) for the winter of 1976–77.

b. Standing eddy variance statistics

In Fig. 14 are shown the distributions of the standing eddy variance of (a) zonal wind $[\overline{u}^{*2}]$ and (b) meridional wind $[\overline{v}^{*2}]$ and of the root- mean-squares (rms) of (c) geopotential height $[\overline{z}^{*2}]^{1/2}$ and (d) temperature $[\overline{T}^{*2}]^{1/2}$ for GFDL analysis (left panel), NMC analysis (middle panel), and the difference between the two sets (right panel).

1) ZONAL AND MERIDIONAL WIND

There are substantial differences in the amplitudes of the deviations of the wind fields from the zonal mean (Figs. 14a and 14b). The standing eddy kinetic energy as estimated by the GFDL set is ~60% of the corresponding NMC values. By making use of the data produced by a GFDL general circulation model, Oort (1978, Fig. 10) also showed that the estimates of the standing eddy kinetic energy based on a simulated rawinsonde network are considerably lower than the corresponding values based on the full model grid.

2) GEOPOTENTIAL HEIGHT

The patterns for the rms of geopotential height (Fig. 14c) are very similar. The largest deviations between the two data sets (up to ~20%) are found at 40°N near the tropopause.

3) TEMPERATURE

The patterns for the rms temperature (Fig. 14d) also exhibit a strong resemblance—the maximum deviations are ~10%. The zonal symmetry of the difference map between the two sets for temperature (Fig. 10c) partially accounts for the good correspondence in the variance statistics.

c. Standing eddy covariance statistics

The meridional transports of (a) zonal momentum $[\overline{v}^*\overline{u}^*]$, (b) geopotential energy $[\overline{v}^*\overline{z}^*]$ and (c) heat $[\overline{v}^*\,\overline{T}^*]$ by the stationary eddies are compared in Fig. 15.

1) MOMENTUM TRANSPORT

As a result of the relatively more intense eastward and northward flows in the NMC wind analyses over the western oceans between 30 and 45°N (Figs. 3c and 5c), the poleward transport of zonal momentum is stronger in the NMC pattern (Fig. 15a). The estimate by the GFDL set on the convergence of standing eddy momentum transports into the middle latitudes at 200 mb is ~75% of the corresponding NMC values. By making use of the NMC analyses and conventional station analyses for January 1964, Holopainen (1968, Table 1) has shown that the former data yield relatively stronger total momentum flux across the 42.5°N latitude at 300 mb. The much stronger momentum transports derived from time-averaging of daily synoptic analyses at the 500 mb level also have been noted by Mak (1978). On the other hand, the study by Rosen and Salstein (1980, Fig. 9) indicates that the estimates of $[\overline{u}^*\overline{v}^*]$ by station analyses for the winter of 1976–77 are higher than those by NMC Hough analyses.

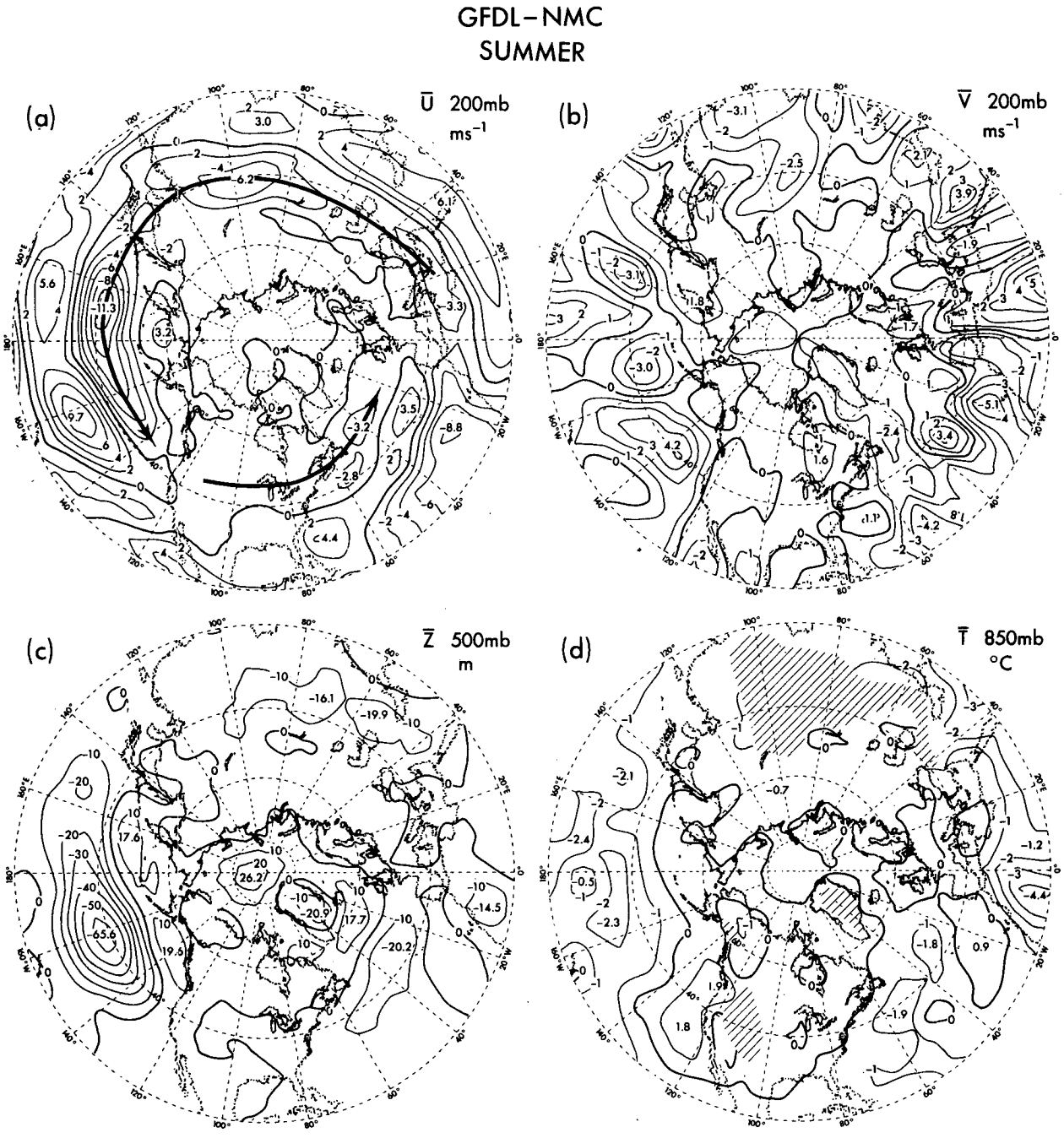

FIG. 12. Difference maps obtained by subtracting the NMC analysis from the corresponding GFDL analysis, based on the 9-summer averages of (a) zonal wind (m s^{-1}) at 200 mb, where the arrows depict the positions of the two principal summertime jet streams as inferred from the NMC analysis, (b) meridional wind (m s^{-1}) at 200 mb, (c) geopotential height (m) at 500 mb and (d) temperature (°C) at 850 mb, where the shaded areas indicate local topographic heights > 1500 m.

2) GEOPOTENTIAL ENERGY TRANSPORT

At some latitudes in the upper troposphere, the GFDL analyses give equatorward transports which are 2–3 times stronger than the NMC results (Fig. 15b). Since $[\bar{v}^* \bar{z}^*] = 0$ for geostrophic flow, this discrepancy is associated with the relatively stronger ageostrophic component in the GFDL wind analyses. The contribution of such ageostrophic effects to the equatorward geopotential energy transport is particularly evident near the stationary troughs over eastern Asia and northern Africa, where $\bar{z}^* <$

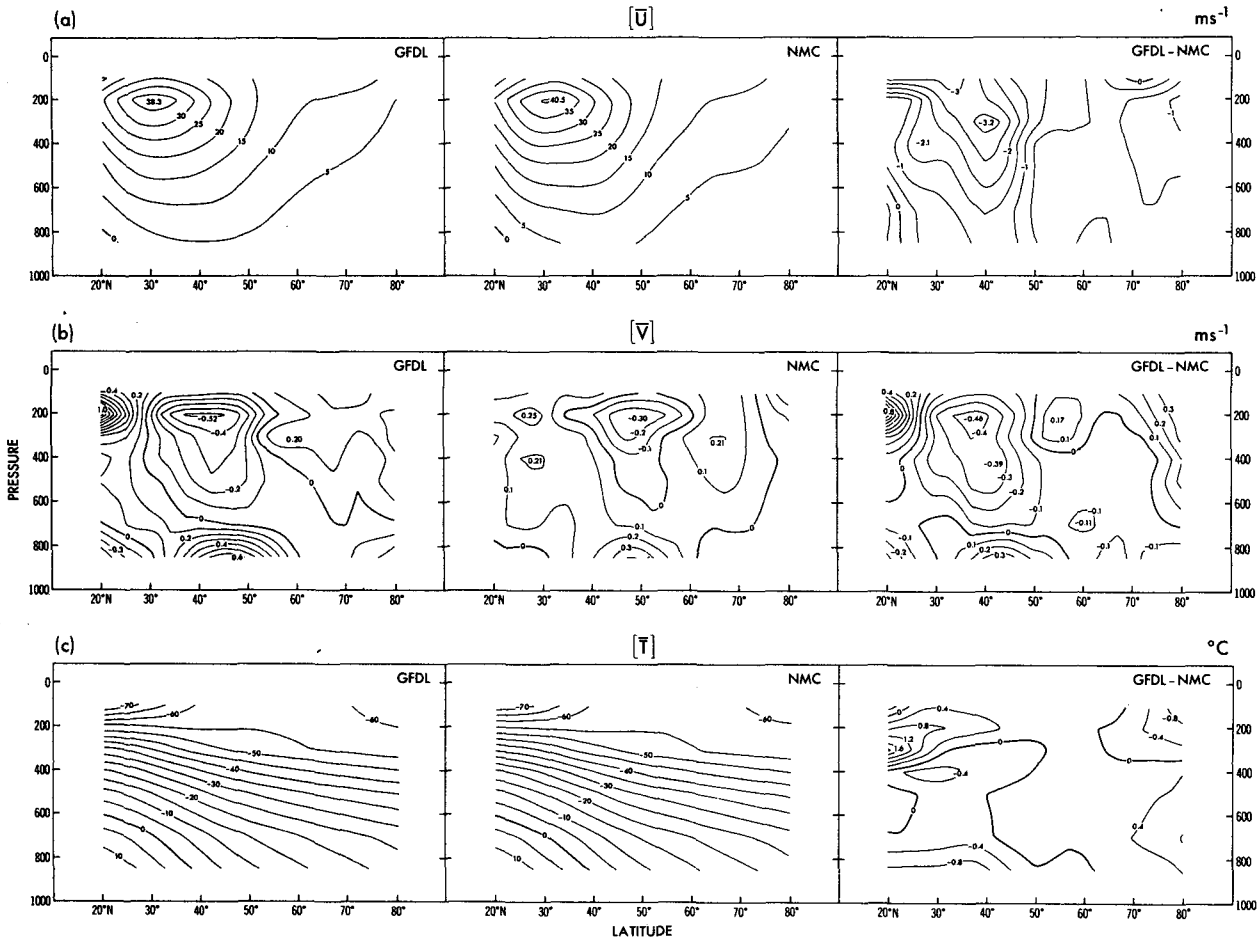

FIG. 13. Meridional cross sections of the zonal mean of (a) zonal wind (m s^{-1}), (b) meridional wind (m s^{-1}), and (c) temperature (°C), based on the 9-winter average of GFDL analysis (left panel) and NMC analysis (middle panel). The differences between the two sets (GFDL minus NMC) are shown in the right panel.

0 and the GFDL analyses give much stronger poleward ageostrophic winds at 200 mb (Fig. 8a).[11]

3) HEAT TRANSPORT

The estimates on standing eddy heat transports by the two data sets are quite similar in the troposphere (Fig. 15c). The largest deviations (~3°C m s^{-1}) occur between 40 and 50°N at 200 mb. The corresponding patterns for the station and NMC Hough analyses during the winter of 1976–77 (Rosen and Salstein, 1980, Fig. 14) also exhibit a strong resemblence. However, during that winter the NMC analyses gave a weaker rather than a stronger poleward standing eddy heat flux near 45°N.

5. Hemispheric distributions of the temporal variability of monthly mean fields

In this section the GFDL and NMC patterns for the standard deviation of monthly mean fields of zonal wind at 200 mb (Fig. 16), geopotential height at 500 mb (Fig. 17) and temperature at 850 mb (Fig. 18) are compared. The seasonal cycle has been removed from the time series of each field by subtracting the 9-year average from each respective calendar month to obtain deviations. All results in this section are based on gridded data of the monthly mean analyses. In presenting these results we wish to gain some appreciation of the geographical dependence of the intermonthly variability depicted by the two data sets. The information in this section may be helpful to observational studies of the atmospheric variability with time scales on the

[11] If the difference between the GFDL and NMC analyses for a quantity X is denoted by $\Delta X \equiv X_{\mathrm{GFDL}} - X_{\mathrm{NMC}}$, then

$$\Delta[\bar{v}^*\bar{z}^*] = [\bar{z}^*_{\mathrm{NMC}}\Delta\bar{v}^*] + [\bar{v}^*_{\mathrm{NMC}}\Delta\bar{z}^*] + [\Delta\bar{v}^*\Delta\bar{z}^*].$$

At 200 mb and 40°N, $\bar{z}^* \approx 200$ m, $\Delta\bar{z}^* \approx 50$–$70$ m, $\bar{v}^* \approx \Delta\bar{v}^* \approx 5$ m s^{-1}; it is evident that $\Delta[\bar{v}^*\bar{z}^*]$ is essentially determined by the first term on the right-hand-side of the above expression.

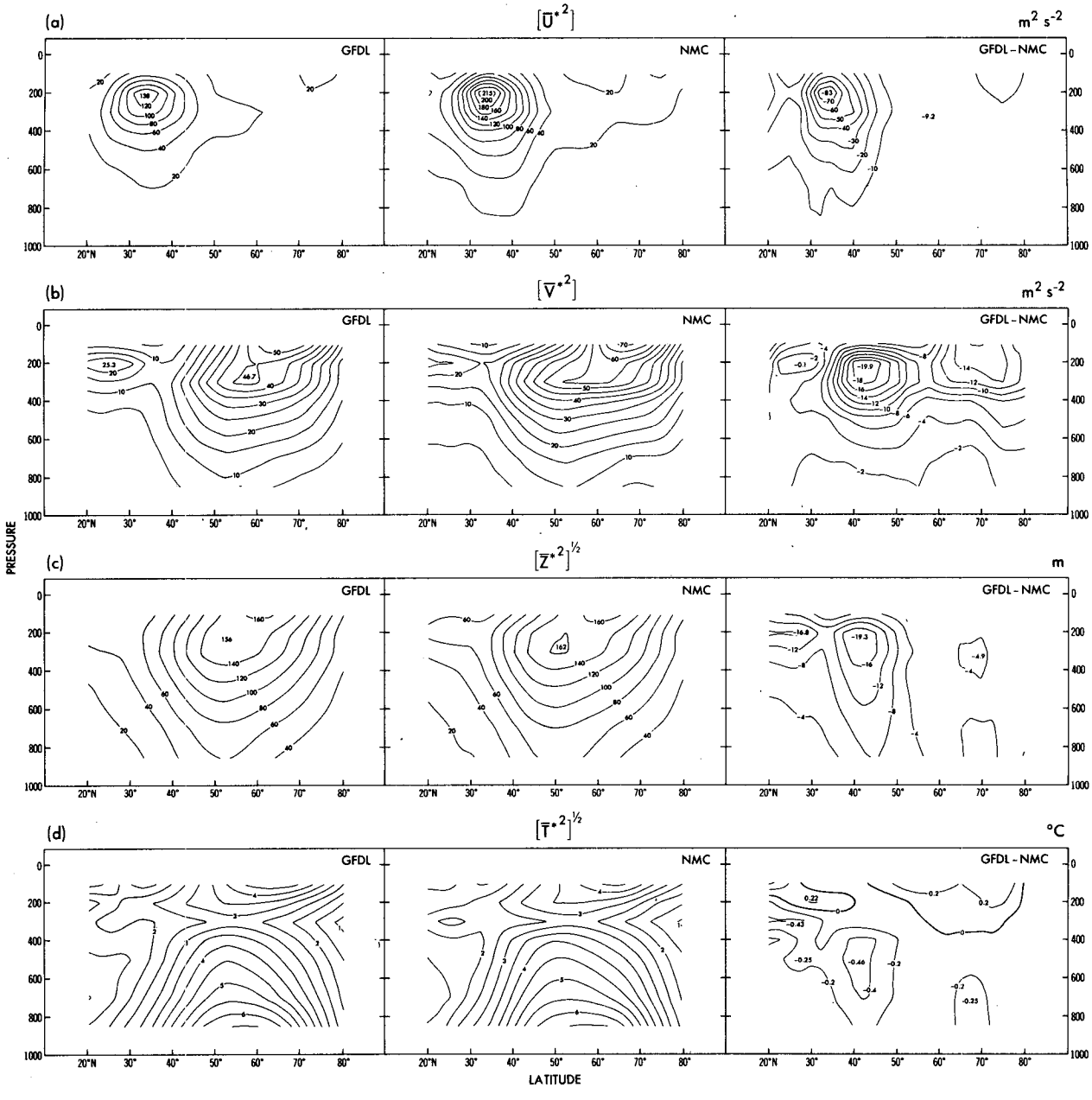

FIG. 14. As in Fig. 13 except for standing eddy variance of (a) zonal wind ($m^2\ s^{-2}$), (b) meridional wind ($m^2\ s^{-2}$), the rms of (c) geopotential height (m) and (d) temperature (°C).

order of months, and to verification of very long-term integrations of general circulation models.

a. Zonal wind

Inspection of Fig. 16 indicates that there exists a good agreement between the GFDL and NMC sets with respect to the month-to-month variability of the 200 mb zonal wind over North America, Europe and northern Asia. However, the variability over the oceans as computed by using GFDL analyses is lower than the corresponding NMC results by as much as 5–8 m s^{-1} over the central Pacific, and by 2–4 m s^{-1} over the Atlantic. For the GFDL pattern (Fig. 16a), the features over the Pacific appear to be linked to the distribution of the few reporting stations in that region, where the centers of maximum variability coincide with the location of Ship V, Midway, Ship P and Ship N (marked by solid dots in Fig. 16a). This is in part responsible for the very different spatial distributions for the two data sets over the Pacific Basin. These remarks also apply to the GFDL patterns for geopotential height (Fig. 17a) and temperature (Fig. 18a) pre-

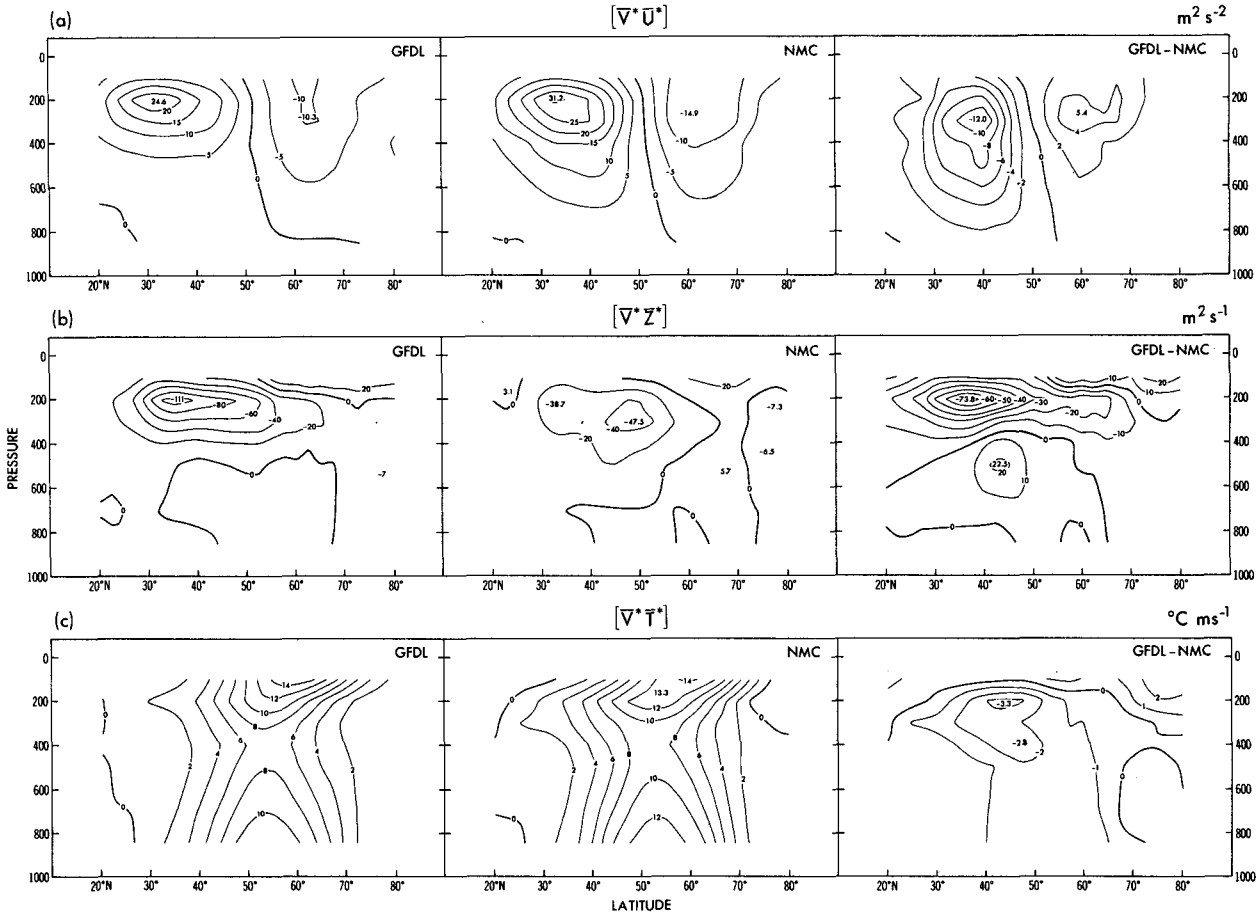

FIG. 15. As in Fig. 13 except for the standing eddy meridional transports of (a) westerly momentum ($m^2 s^{-2}$), (b) geopotential energy ($m^2 s^{-1}$) and (c) heat (°C m s^{-1}).

sented in the following subsections. These latter patterns similarly indicate the influences of the data input from Ship V and Midway in an extensive data-sparse region.

b. *Geopotential height*

The GFDL and NMC patterns for the standard deviations of the monthly mean geopotential height field at 500 mb also compare well over much of the continental regions (Fig. 17). The largest differences are located over the Pacific and Northern Atlantic, where the standard deviations given by the GFDL analyses are lower by as much as 40–60 m and 10–30 m, respectively.

c. *Temperature*

The patterns for the variability of the temperature field at 850 mb appear to be largely similar for the two data sets (Fig. 18). The largest discrepancies are found over parts of the Pacific and Atlantic, as well as over the Arctic region, where the monthly means in the GFDL set are relatively less variable.

6. Temporal variations of the spatial correlations between the GFDL and NMC patterns

During the 9-winter period covered by the present study, substantial changes were made in various components of the analysis system for the NMC data set. Most of those changes are associated with the numerics of the NMC forecast models and the use of bogus data. For the GFDL set, the data handling and analysis procedures are uniform throughout the entire period. However, for both the NMC and GFDL sets there are changes associated with variation in the density of the observational network. The total impact of all these changes on the spatial correspondence of the GFDL and NMC patterns may be evaluated by examining the time series of the correlation coefficients[12] between the two

[12]For the variable X and the month k, the spatial correlation coefficient between the GFDL and NMC analyses is given by

$$R^k(X) = \frac{\sum_{i,j} (X^{ijk}_{\mathrm{GFDL}}\, g^j - \tilde{X}^k_{\mathrm{GFDL}})\,(X^{ijk}_{\mathrm{NMC}}\, g^j - \tilde{X}^k_{\mathrm{NMC}})}{\left[\sum_{i,j} (X^{ijk}_{\mathrm{GFDL}}\, g^j - \tilde{X}^k_{\mathrm{GFDL}})^2\right]^{1/2} \cdot \left[\sum_{i,j} (X^{ijk}_{\mathrm{NMC}}\, g^j - \tilde{X}^k_{\mathrm{NMC}})^2\right]^{1/2}}$$

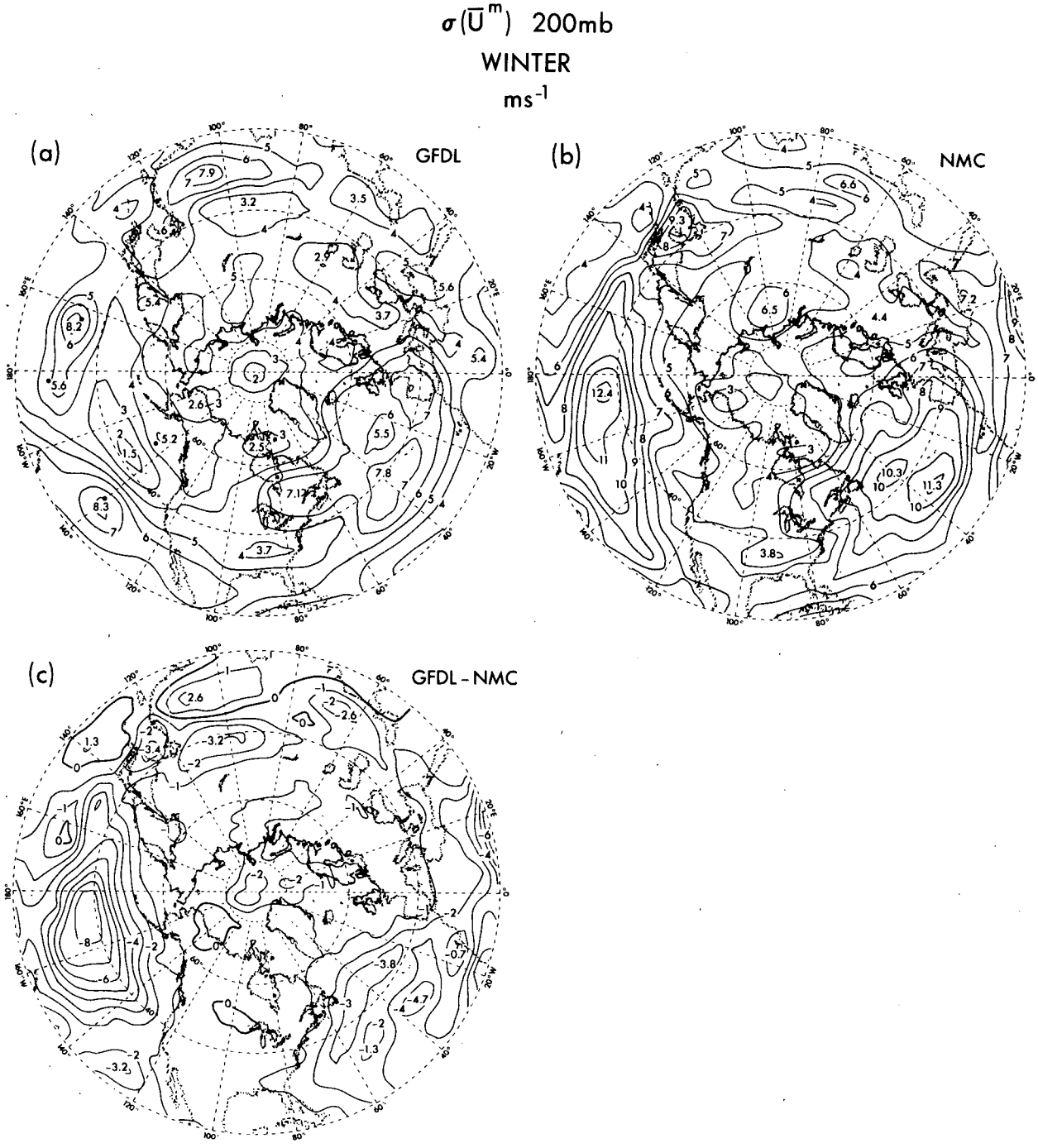

FIG. 16. Wintertime distributions of the standard deviation of monthly means of zonal wind (m s^{-1}) at 200 mb, based on (a) GFDL analysis and (b) NMC analysis. The corresponding difference map between the two sets (GFDL minus NMC) is shown in (c). The dots in (a) indicate the locations of the reporting rawinsonde stations over the central and eastern Pacific.

where $\tilde{X}^k = S^{-1} \sum_{i,j} X^{ijk} g^j$, $S = \sum_{i,j} g^j$, X^{ijk} is the value at the grid point with longitude i and latitude j in month k. The summations are performed over the domain from 20 to 90°N. The data at latitude θ^j are weighted by $g^j = \cos\theta^j$.

patterns for a given field. With the exception of the meridional velocity field, the spatial correlation coefficients (not shown) between the monthly mean patterns for the two data sets tend to be uniformly high throughout the 9-winter seasons. There exists

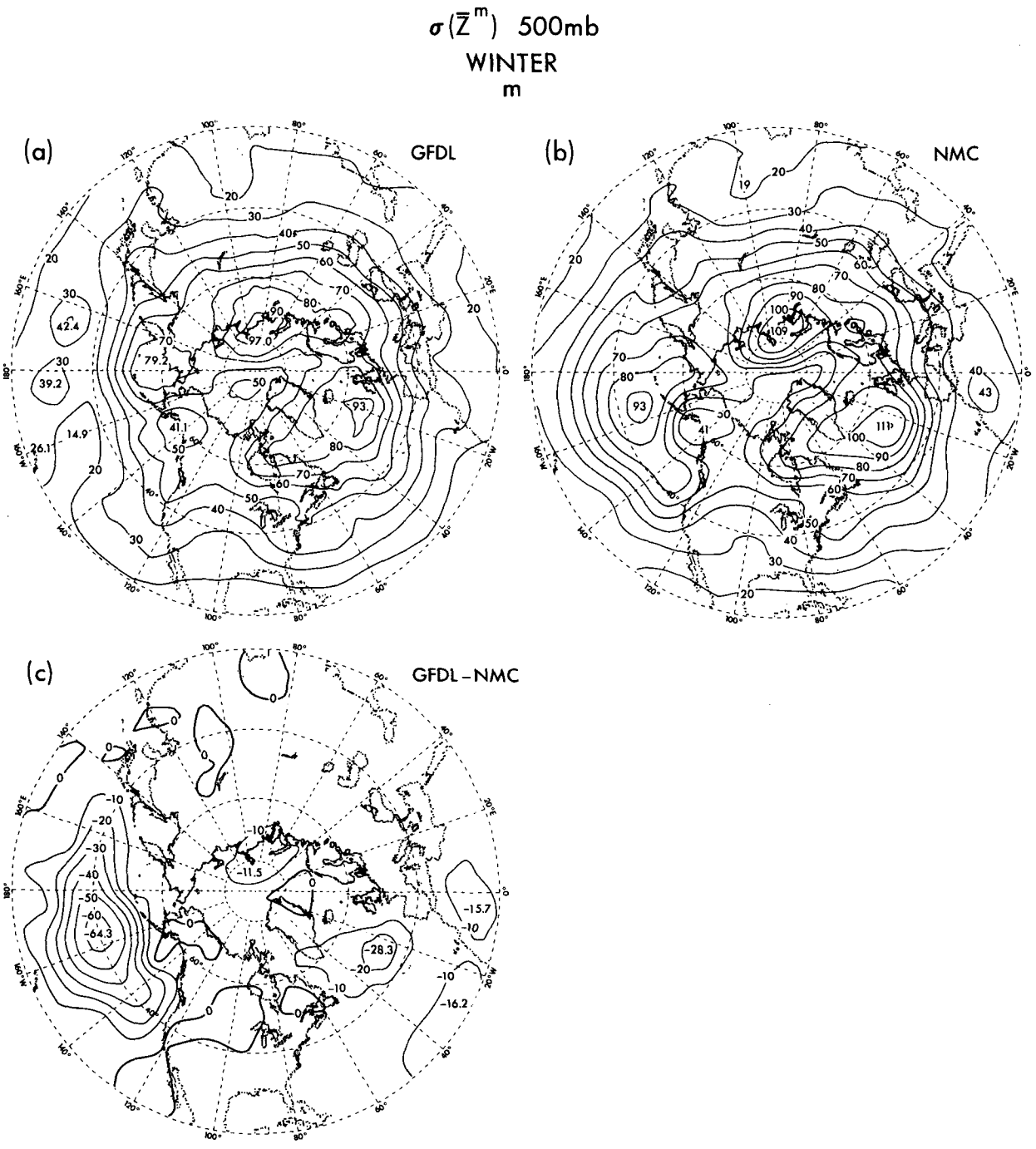

FIG. 17. As in Fig. 16 except for geopotential height (m) at 500 mb.

no clear evidence of any discernible trends in the spatial correlations during this period. The correlation coefficients between the GFDL and NMC patterns in various months range from 0.949 to 0.985 for zonal wind at 200 mb, from 0.741 to 0.930 for meridional wind at 200 mb, from 0.986 to 0.998 for geopotential height at 500 mb, and from 0.978 to 0.996 for temperature at 850 mb.

The temporal variations of the spatial correlation between monthly anomalies (i.e., departures from the long-term mean) appearing in the two sets may be studied in a similar manner. For this purpose, the 9-year average is subtracted from each respective calendar month before the spatial correlation coefficients are computed. In Fig. 19 are shown the time series of the correlation coefficients between

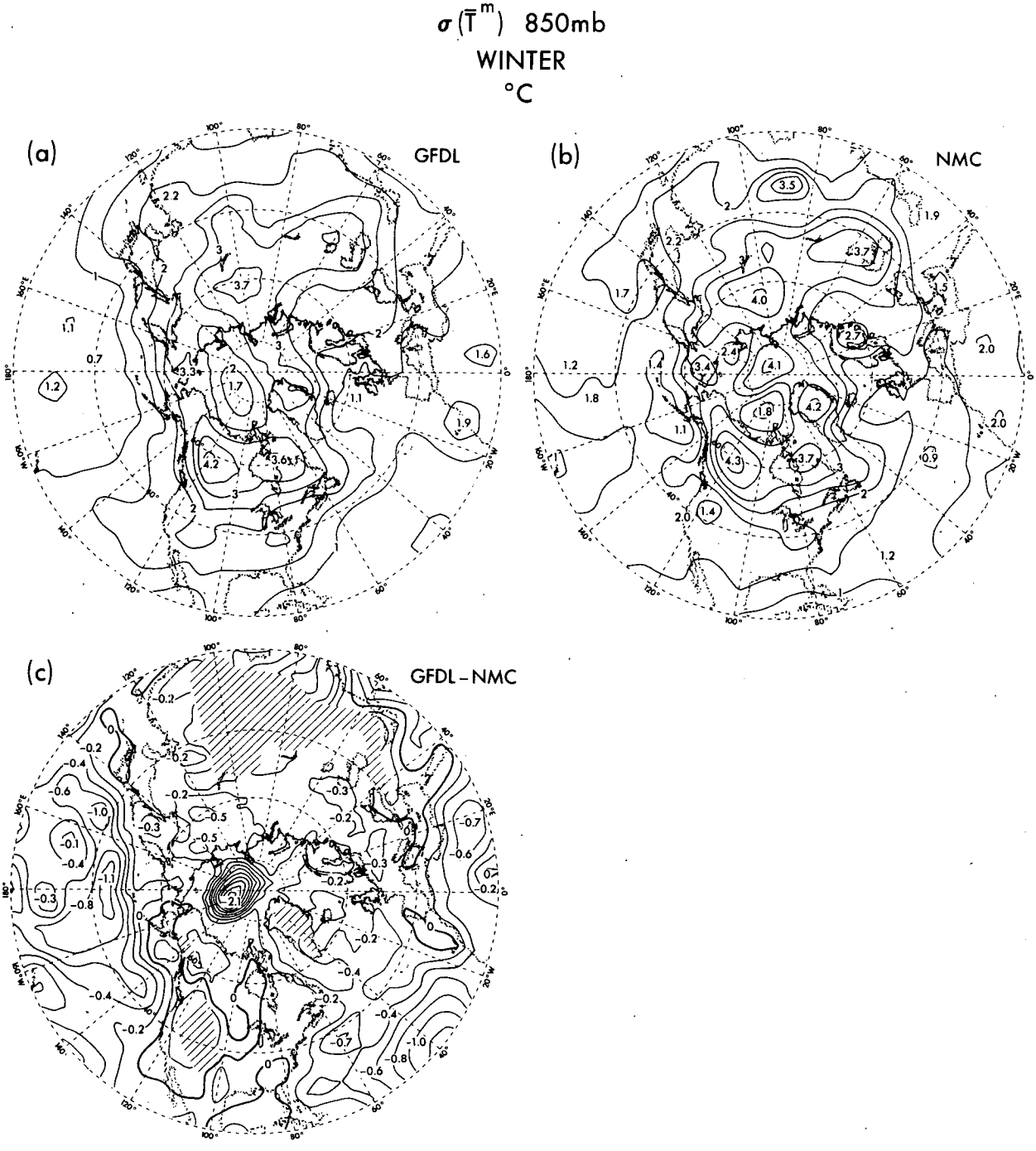

FIG. 18. As in Fig. 16 except for temperature (°C) at 850 mb. The shaded areas in (c) indicate local topographic heights > 1500 m.

the anomaly patterns given by the GFDL and NMC analyses for the four variables discussed in Section 3. It is seen that the correlation coefficients for monthly anomalies are generally lower than the corresponding values for monthly means. The range of the variations in the former is also relatively wider. Inspection of Fig. 19 further reveals no significant trend during the 9-winter period. Only in the case of $\bar{u}$ and $\bar{v}$ is there a weak tendency for higher correlations during the later years.

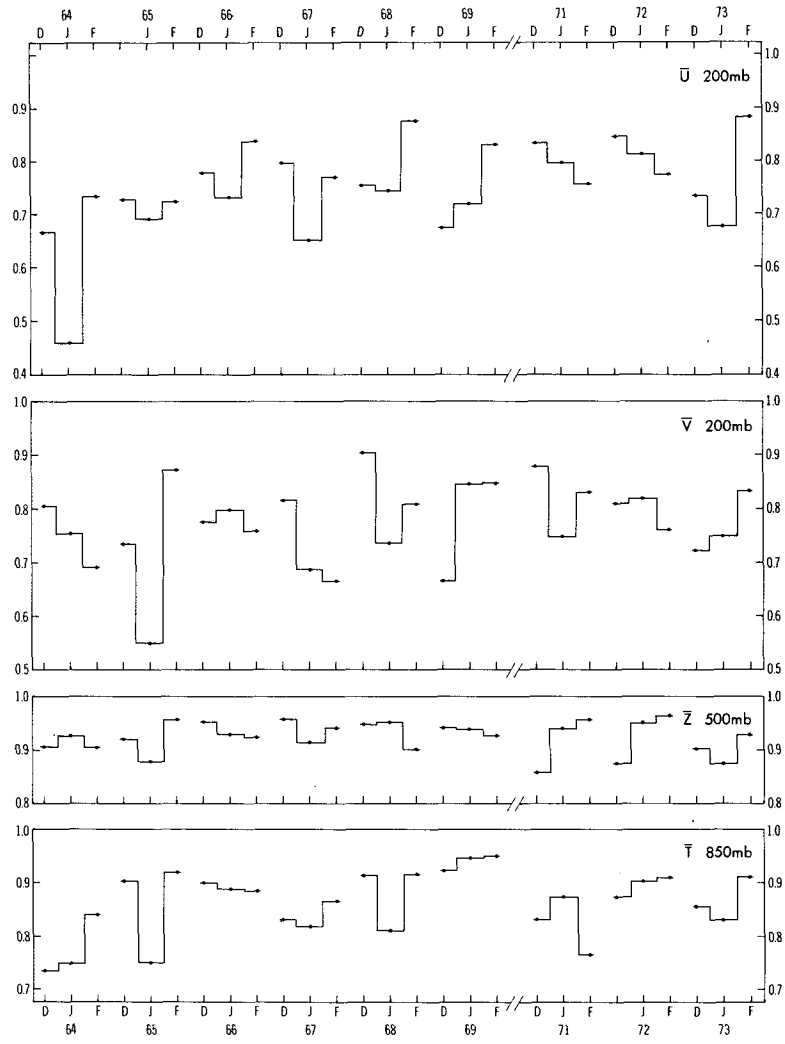

FIG. 19. Time series of spatial correlation coefficients between contemporaneous monthly anomaly patterns of the GFDL and NMC analyses for zonal wind at 200 mb, meridional wind at 200 mb, geopotential height at 500 mb, and temperature at 850 mb.

7. Discussion

It should be emphasized that, on the basis of the present comparison, it is not possible to decide which set of analyses is better than the other. The inferences to be drawn here are of necessity somewhat tentative and subjective. Judging from the findings presented so far, it is felt that the following assessment of the relative merits of the GFDL and NMC data sets may be made:

- The GFDL data set tends to underestimate the strength of the zonal flow in the jet exit regions over the middle Pacific and middle Atlantic. We reach this conclusion in view of the fact that the zonal wind speed maxima in the GFDL data set are considerably weaker than the corresponding values reported by rawinsonde stations located in these regions (Fig. 3d). This notion is reinforced by some unpublished results using the history tapes of a general circulation model developed at GFDL and described by Manabe and Holloway (1975). By adopting the methodology outlined in Oort (1978), these results indicate that the estimates of the zonal wind speeds over the oceans based on a simulated observing network reflecting the realistic distribution of rawinsonde stations are weaker than the corresponding values based on the full model grid by up to 10–15 m s^{-1}. Associated with this underestimate of zonal wind speeds over the oceans is the relatively weaker standing eddy kinetic energy in the GFDL data set (Fig. 14a).
- As a result of the systematic bias of the NMC

wind analyses toward gradient wind balance over the data-sparse areas, the corresponding estimates on parameters related to ageostrophic processes are less realistic. These include the time-averaged meridional wind (Fig. 5), intensity of the mean meridional circulation (Fig. 13b), and the meridional transport of geopotential energy (Fig. 15b).

• In view of the noticeable effects of the geographical locations of reporting stations over the Pacific on the GFDL patterns for standard deviations of the monthly means (Figs. 16a, 17a and 18a), the features in these patterns over that region would probably be altered if there existed a better observing network. The corresponding impact of such changes on the NMC analyses would be less localized.

A principal contributing factor to the suppressed variability in the GFDL analyses at the data gaps over the oceans is the choice of the zonal mean as the first-guess field, since zonally averaged statistics are generally less variable than the corresponding local values. This difficulty may be partially overcome by first computing the standard deviations at individual stations using monthly averaged rawinsonde data (as opposed to computing the standard deviations using interpolated monthly mean data at latitude-longitude intersections), and then interpolating the station values onto a regular grid. This approach has been adopted in the atlas compiled by Oort (1981).[4] The resulting patterns over the oceans are spatially more uniform, although the magnitude of the variability over these regions is still lower than that in the NMC analyses.

In Part II of this study, the two sets of analyses will be compared in terms of the daily variability of selected meteorological variables and the transport characteristics of transient eddies. The differences between the two data sets in the stationary and transient aspects of the general circulation will then be examined within the framework of the atmospheric energy cycle.

Acknowledgments. We would like to thank Drs. E. O. Holopainen, J. D. Mahlman, S. Manabe, K. Miyakoda, R. D. Rosen and J. M. Wallace for their helpful comments on the manuscript, Mr. R. L. Jenne and his associates at NCAR for their cooperation in providing the monthly mean NMC analyses, and Messrs. W. Ellis and P. Tunison at GFDL for drafting the figures. NCL is supported by a Visiting Scientist appointment at the Geophysical Fluid Dynamics Program, through NOAA Grant 04-7-022-44017.

REFERENCES

Blackmon, M. L., 1976: A climatological spectral study of the 500 mb geopotential height of the Northern Hemisphere. *J. Atmos. Sci.*, **33**, 1607–1623.

——, and N-C. Lau, 1980: Regional characteristics of the Northern Hemisphere wintertime circulation: a comparison of the simulation of a GFDL general circulation model with observations. *J. Atmos. Sci.*, **37**, 497–514.

——, J. M. Wallace, N-C. Lau and S. L. Mullen, 1977: An observational study of the Northern Hemisphere wintertime circulation. *J. Atmos. Sci.*, **34**, 1040–1053.

Brown, J. A., 1964: A diagnostic study of tropospheric diabatic heating and the generation of available potential energy. *Tellus*, **16**, 371–388.

Clapp, P. F., 1956: Some considerations involved in preparing long range weather forecasts by numerical methods. *J. Meteor.*, **13**, 341–350.

Cressman, G. P., 1959: An operational objective analysis system. *Mon. Wea. Rev.*, **87**, 367–374.

Geller, M. A., and S. K. Avery, 1978: Northern Hemisphere distributions of diabatic heating in the troposphere derived from general circulation data. *Mon. Wea. Rev.*, **106**, 629–636.

Haines, D. A., and J. S. Winston, 1963: Monthly mean values and spatial distribution of meridional transport of sensible heat. *Mon. Wea. Rev.*, **91**, 319–328.

Holopainen, E. O., 1968: A note on the use of a forecast as the first guess in objective analyses. *Tellus*, **20**, 129–131.

——, 1978a: A diagnostic study of the kinetic energy balance of the long-term mean flow and the associated transient fluctuations in the atmosphere. *Geophysica*, **15**, 125–145.

——, 1978b: On the dynamic forcing of the long-term mean flow by the large-scale Reynolds' stresses in the atmosphere. *J. Atmos. Sci.*, **35**, 1596–1604.

Klein, W. H., 1951: A hemispheric study of daily pressure variability at sea level and aloft. *J. Meteor.*, **8**, 332–346.

Krueger, A. F., J. S. Winston and D. A. Haines, 1965: Computations of atmospheric energy and its transformation for the Northern Hemisphere for a recent five-year period. *Mon. Wea. Rev.*, **93**, 227–238.

Lau, N-C., 1978: On the three-dimensional structure of the observed transient eddy statistics of the Northern Hemisphere wintertime circulation. *J. Atmos. Sci.*, **35**, 1900–1923.

——, 1979a: The structure and energetics of transient disturbances in the Northern Hemisphere wintertime circulation. *J. Atmos. Sci.*, **36**, 982–995.

——, 1979b: The observed structure of tropospheric stationary waves and the local balances of vorticity and heat. *J. Atmos. Sci.*, **36**, 996–1016.

——, and J. M. Wallace, 1979: On the distribution of horizontal transports by transient eddies in the Northern Hemisphere wintertime circulation. *J. Atmos. Sci.*, **36**, 1844–1861.

——, G. H. White and R. L. Jenne, 1981: Circulation statistics for the extratropical Northern Hemisphere based on NMC analyses. NCAR Tech. Note NCAR/TN-171 + STR.

Mak, M., 1978: On the observed momentum flux by standing eddies. *J. Atmos. Sci.*, **35**, 340–346.

Manabe, S., and J. L. Holloway, Jr., 1975: The seasonal variation of the hydrologic cycle as simulated by a global model of the atmosphere. *J. Geophys. Res.*, **80**, 1617–1649.

Namias, J., and P. F. Clapp, 1949: Confluence theory of the high tropospheric jet stream. *J. Meteor.*, **6**, 330–336.

Newell, R. E., J. W. Kidson, D. G. Vincent and G. J. Boer, 1972 and 1974: *The General Circulation of the Tropical Atmosphere and Interactions with Extratropical Latitudes*, Vols. 1 and 2. The MIT Press, 258 and 371 pp.

Oort, A. H., 1978: Adequacy of the rawinsonde network for global circulation studies tested through numerical model output. *Mon. Wea. Rev.*, **106**, 174–195.

——, and E. M. Rasmusson, 1971: *Atmospheric Circulation Statistics*. NOAA Prof. Paper 5, U.S. Government Printing Office, Washington, DC [NTIS COM-72-50295].

——, and J. P. Peixóto, 1974: The annual cycle of the energetics of the atmosphere on a planetary scale. *J. Geophys. Res.*, **79**, 2705–2719.

——, and ——, 1976: On the variability of the atmospheric energy cycle within a 5-year period. *J. Geophys. Res.*, **81**, 3643–3659.

——, and T. H. vonder Haar, 1976: On the observed annual cycle in the ocean-atmosphere heat balance over the Northern Hemisphere. *J. Phys. Oceanogr.* **6**, 781–800.

——, and P. H. Chan, 1977: On the role of the Asian monsoon in the angular momentum and kinetic energy balances of the tropics. *Pure Appl. Geophys.*, **115**, 1167–1186.

Peixóto, J. P., and A. H. Oort, 1974: The annual distribution of atmospheric energy on a planetary scale. *J. Geophys. Res.*, **79**, 2149–2159.

——, R. D. Rosen and D. A. Salstein, 1978: Seasonal variability in the pole-to-pole modes of water vapor transport during the IGY. *Arch. Meteor. Geophys. Biolim.*, **A27**, 233–255.

Rosen, R. D., and D. A. Salstein, 1980: A comparison between circulation statistics computed from conventional data and NMC Hough analyses. *Mon. Wea. Rev.*, **108**, 1226–1247.

Shuman, F. G., and J. B. Hovermale, 1968: An operational six-layer primitive equation model. *J. Appl. Meteor.*, **7**, 525–547.

Trenberth, K. E., 1979: Interannual variability of the 500 mb zonal mean flow in the Southern Hemisphere. *Mon. Wea. Rev.*, **107**, 1515–1524.

Van Loon, H., R. L. Jenne and K. Labitzke, 1973: Zonal harmonic standing waves. *J. Geophys. Res.*, **78**, 4463–4471.

Wiin-Nielsen, A., 1959: A study of energy conversion and meridional circulation for the large-scale motion in the atmosphere. *Mon. Wea. Rev.*, **87**, 319–332.

——, J. A. Brown and M. Drake, 1963: On atmospheric energy conversions between the zonal flow and the eddies. *Tellus*, **15**, 261–279.

——, —— and ——, 1964: Further studies of energy exchanges between the zonal flow and the eddies. *Tellus*, **16**, 168–180.